A&A 385, 181–204 (2002)
DOI: 10.1051/0004-6361:20020058

Astronomy & Astrophysics

Radial mixing in protoplanetary accretion disks

II. Time dependent disk models with annealing and carbon combustion

M. Wehrstedt and H.-P. Gail

Institut für Theoretische Astrophysik, Universität Heidelberg, Tiergartenstraße 15, 69121 Heidelberg, Germany
e-mail: gail@ita.uni-heidelberg.de

Received 12 November 2001 / Accepted 14 January 2002

Abstract. This work investigates the annealing of silicate dust, the combustion of carbon dust and radial mixing of both dust species within protoplanetary disks. For this purpose the diffusion-transport-reaction equations of both dust species (including annealing of silicate and carbon combustion) are simultaneously solved with the equations for the global evolution of an α-disk within an one-zone, time-dependent numerical model. The protostar-disk system is assumed to be in a quiescent stage which corresponds with the class II phase of evolution of star-disk systems. The results suggest that the diffusive transport spreads the dust globally throughout the disk, and therefore provides an explanation for the existence of crystalline silicate and methane within the primordial bodies of the solar system.

Key words. accretion, accretion disks – solar system: formation – comets: general – dust, extinction

1. Introduction

IR-spectra of many comets show clear evidence for the presence of crystalline silicate dust (predominantly olivine) in notable quantities, besides the well known features of amorphous silicate dust (Hanner et al. 1994a; Hanner et al. 1994b; Crovisier et al. 1997; Hanner et al. 1997; Yanamandra-Fisher & Hanner 1999). It is generally assumed that the matter in cometary nuclei represents unaltered pristine material from the time of formation of the solar nebula, which has been "frozen in" since its integration into cometesimals. Since the dust in the interstellar medium is exclusively amorphous, the protoplanetary accretion disk itself must be the formation site of the crystalline silicate. A possible formation process is annealing of amorphous silicate in the warm inner zone of the accretion disk. Due to diffusional mixing induced by turbulence in the optically thick disk, a fraction of the annealed silicate dust arrives at the cooler outer region of the disk, where it may be built into larger bodies, e.g. cometesimals. In the matrix material of some chondrites there are also indications for the presence of silicate dust, which has experienced an annealing-event under the conditions of the solar nebula. The process of radial mixing also is assumed to be responsible for the existence of methane in comets (e.g. Crovisier & Bockelée-Morvan 1999a).

Send offprint requests to: M. Wehrstedt,
e-mail: mwehrste@ita.uni-heidelberg.de

The idea of turbulent radial mixing of tracers across wide ranges of the protoplanetary disk is attributed to Morfill (1983). The following papers discuss and refine this idea: Morfill & Völk 1984; Morfill 1985; Morfill et al. 1985). These investigations, however, solely include the calculation of simple analytical disk models. For a different type of a simple analytical disk model Stevenson & Lunine (1988) examined, by numerically solving the diffusion equation, the radial mixing of water vapour in the disk. For solving the diffusion-transport-reaction equation in one dimension, they assumed $v_r = -D/r$ in order to simplify the advection term, and moreover they employed a simple $T_c \propto r^{-1}$ law for the radial temperature structure of the disk. Here v_r denotes the radial advection velocity, D the diffusion coefficient of the tracer in the disk gas and T_c the temperature in the midplane of the disk, respectively. In addition, Stevenson (1990) obtained an analytical solution of the diffusion-transport-reaction equation for the diffusion of trace molecules, but again for a simple approximation for the disk structure.

On the basis of a numerical solution of the diffusion equation for the concentration of a tracer, Cyr et al. (1998) calculated the radial mixing of water vapour by applying the semi-analytical model of Cassen (1994) for the disk structure, and compared their results with that of Stevenson & Lunine (1988). Another numerical model is that of Drouart et al. (1999), who calculated the radial mixing of deuterium in the solar nebular. They used the analytical model of Dubrulle (1993) for the disk structure,

which includes the more realistic approach for the opacity law from Ruden & Pollack (1991), but the model did not include the solution of the time dependent equation for the conservation of angular momentum in the disk.

In the first part of the present series (Gail 2001a, henceforth called Paper I) stationary numerical models of protoplanetary accretion disks have been calculated which consider the combustion of carbon dust, annealing of silicate dust and radial mixing of the dust species. As shown in Paper I, carbon combustion, annealing of silicates and radial mixing have considerable influence on the chemical composition of the disk matter as well as on the radial disk structure. Stationary models, however, have an only limited value since the lifetime of protoplanetary disks of about 10^7 yr (Strom et al. 1993) is less than the diffusion timescale in the outer parts of the disk. Because of the importance of radial mixing with respect to the composition of the primordial bodies in the solar system (and other planetary systems) time dependent models are required for a realistic treatment of mixing processes.

In this paper for the first time an attempt is made to obtain numerically simultaneous solutions of both, the equation of the conservation of angular momentum (including a set of equations for the disk structure in the one-zone approximation), and two sets of diffusion-transport-reaction equations for the concentration of tracers in the one-zone approximation. The tracers considered are silicate dust grains which are converted from amorphous to crystalline grains by annealing and solid carbon grains which are oxidised by OH molecules. The purpose of this work is to extend the discussion of Duschl et al. (1996), Gail (1998) and Paper I of the impact of annealing of amorphous silicates and of the destruction of carbon by combustion on the structure of protoplanetary disks, and to improve previous model calculations by calculating time dependent models.

Observational evidence for both annealing of silicate and for carbon combustion in the early stage of the solar system can be seen in the comets. At one hand IR spectra of many comets exhibit prominent features in the region of the 10 μm silicate band, which can be explained by the presence of a substantial fraction of crystalline silicates in these comets (Hanner et al. 1994a; Hanner et al. 1994b; Crovisier et al. 1997; Hanner et al. 1997; Yanamandra-Fisher & Hanner 1999). On the other hand, a large abundance of methane is observed in comets (Crovisier & Bockelée-Morvan 1999a). In both cases no possible process of formation at small temperatures is known, i.e. the temperature in the region of formation of the comets within the primordial nebula was too low to form appreciable quantities of crystalline silicate and of CH_4. Thus, we assume that the formation processes of crystalline dust and methane occur in warmer parts of the primordial nebula and, after their formation, the products are carried around by turbulent eddies and are mixed to the location of formation of the comets afar from the protostar. In case of crystalline silicate grains the formation process is supposed to be annealing. In case of methane we refer to Finocchi et al. (1997a) who proposed a chain of follow-up reactions of the products of carbon combustion which forms a number of hydrocarbons like CH_4.

The model calculations of the present paper are for protoplanetary disks in the quiescent evolutionary stage after formation of the star-disk system and before dispersion of the disk by the protostellar wind, which are generally denoted as Class II objects (Natta 2000). The quiescent phase is characterised by the global transport of angular momentum in the disk, the slow continuous depletion of the disk through the accretion flow onto the protostar, a modest infall of matter onto the disk from the ambient molecular cloud and no sudden violent interruptions in the disk evolution such as thermal or gravitational instabilities, respectively.

Actually, it is currently not known, whether an overall turbulence in the disk drives the accretion process during the whole quiescent phase of the disk evolution. If planetary bodies are rapidly formed, an overall turbulence in the disk might be prevented by emptied rings along the planetary orbits. This would effect the angular momentum transport, i.e. the global evolution of the disk, as well as the radial diffusive mixing of matter within the disk. Since mixing across gaps is impossible our calculation refers to the early disk evolution before gaps are opened by the formation of massive planets.

The organisation of the paper is as follows: Sect. 2 describes the processes of carbon combustion, annealing and radial mixing in the disk, and presents the method of solving the diffusion-transport-reaction equation. Section 3 presents the relevant equations for calculating the disk structure, particularly the opacity law. Section 4 introduces the parameters and boundary conditions of the model calculations. Section 5 presents the results and, finally, Sect. 6 gives our conclusions.

2. Radial mixing in the disk by advective and diffusive transport

This section serves as a summary of Sects. 2–4 in Paper I, containing the relevant equations and assumptions for treating the processes of the combustion of carbon, annealing of silicate and radial mixing within the disk.

2.1. Carbon combustion

First we consider the combustion of solid carbon due to surface reactions with OH molecules. Carbon is one of the most important absorbers in the disks, hence important for the disk's structure. Thus one needs to know the physical process(es) which destroy the solid carbon particles. One might be tempted to conclude that vaporization is the process which destroys solid carbon, as this seems to be a good assumption for at least the other main dust absorbers. However, in protoplanetary disks combustion by OH is the by far more efficient "destroyer" of the solid carbon owing to the sufficient abundance of OH in medium

temperature ranges of the disk (details in Duschl et al. 1996; Finocchi et al. 1997a).

The basic chemical reaction step for carbon oxidation is:

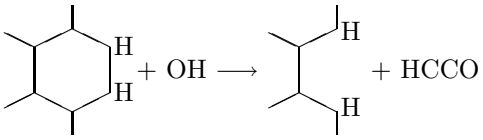

An OH molecule breaks an aromatic six-ring at the surface of the carbon grain and a HCCO radical is injected into the gas phase. It is assumed that carbon dust consists of a conglomerate of such six-rings, and does not appear in the form of meteoritical kerogen which consists of aromatic ring systems bridged by $–CH_2–$ or $–CH_2–O–CH_2–$ groups, quite similar to coal (Anders & Kerridge 1988). As well, we assume no occurrence of graphite or even of diamond.

Of interest also is the chain of subsequent reactions in the disk's gas under medium temperature conditions, starting with the HCCO radical from the above reaction and terminating at CH_4 and finally at CO amongst other products of carbon combustion. The methane might be mixed into the outer zones of the disk by turbulent diffusion and be incorporated there into the growing bodies of the solar system. Hence, carbon combustion and radial mixing possibly explain the large abundance of methane and other hydrocarbons in comets. Some preliminary results for stationary disk models are presented in Gail 2001b (Paper III of this series).

The equation for the change of the radius of a spherical carbon particle by OH combustion is (cf. Eq. (17) of Paper I)

$$\frac{\mathrm{d}a}{\mathrm{d}t} = V_{0,\mathrm{car}} \alpha_{\mathrm{ox}} n_{\mathrm{OH}} v_{\mathrm{th,OH}}. \tag{1}$$

$V_{0,\mathrm{car}}$ is the volume of a carbon atom in solid carbon,

$$V_{0,\mathrm{car}} = \frac{A_{\mathrm{C}} m_{\mathrm{H}}}{\rho_{\mathrm{car}}}, \tag{2}$$

where A_{C} is the atomic weight of carbon, m_{H} the mass of a hydrogen atom and $\rho_{\mathrm{car}} = 2.26\,\mathrm{g\,cm^{-3}}$ the mass density of solid carbon, respectively. α_{ox} represents a probability factor for both the collision and reactions of an OH molecule with the C–C bonds at the grain's surface, which here is chosen to be 0.1 (from laboratory data as discussed in Finocchi et al. 1997a). n_{OH} is the particle density of OH in the disk. With respect to the calculation of n_{OH} we assume that the O–H-chemistry in the region, where oxidation reactions occur, is in chemical equilibrium (Finocchi et al. 1997a; Finocchi & Gail 1997b). Finally we have the root mean square velocity of the OH molecules

$$v_{\mathrm{th,OH}} = \sqrt{\frac{k_{\mathrm{B}} T_{\mathrm{c}}}{2\pi m_{\mathrm{OH}}}}, \tag{3}$$

where k_{B} is the Boltzmann constant, T_{c} the temperature in the midplane of the disk and m_{OH} the mass of the OH molecule, respectively. Actually, oxidation reactions at the surfaces of carbon grains do not only occur at or close to the midplane of the disk, but also at larger heights above the midplane, where the temperature is lower than T_{c} and where the particle density n_{OH} is lower as compared to the density close to the midplane. In view of the unresolved z direction in our model and in order to simplify matters we take the density of OH at the disk's midplane and refer to the discussion in Sect. 3.1 of Paper I for a justification of this.

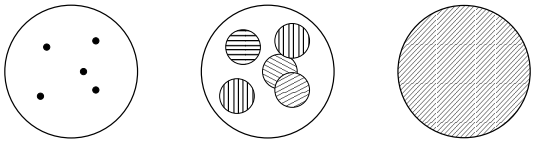

Fig. 1. Illustration of the process of annealing. *Left:* amorphous silicate grain with some small crystalline centers of nucleation. *Middle:* the centers are growing due to annealing. *Right:* the grain is completely crystallised.

We introduce a set of discrete radii a_i ($i = 1 \ldots M$) for the carbon grains. From Eqs. (1) and (3) one obtains the characteristic time of decrease of the radius of carbon grains due to oxidation by OH molecules from radius grid-point a_i to grid-point a_{i+1},

$$\tau_{i,i+1,\mathrm{car}} = \frac{a_i - a_{i+1}}{V_{0,\mathrm{car}} a_{\mathrm{ox}} n_{\mathrm{OH}}} \sqrt{\frac{2\pi m_{\mathrm{OH}}}{k_{\mathrm{B}} T_{\mathrm{c}}}}. \tag{4}$$

Note that the main agent of destruction of carbon particles is not a high temperature, as it is in case of vaporization, but is a high particle density of OH. The carbon released in the oxidation process ultimately will be bound into CO in the oxygen rich environment of the disk, and will not form solid carbon again.

2.2. Annealing of silicate dust

Next we determine an equation for the timescale of annealing of silicate dust particles. We assume that the silicate grains from the parent molecular cloud, which fall onto the disk, are amorphous, i.e. the lattice structure within the solid is characterised by a global disorder of the single atomic building blocks (SiO_4 tetrahedrons). If the temperature is high enough ($T \gtrsim 800\,\mathrm{K}$ under conditions in protoplanetary disks; Duschl et al. 1996), rearrangement processes in the lattice on a big scale begin to occur and finally lead to a crystalline lattice structure. This is a well-known process in material science and is called *annealing*.

Annealing of silicate dust has a large effect on the structure of protoplanetary disks (Paper I). This is traced back to the fact that the opacity of crystalline silicates is an order of magnitude lower than the opacity of amorphous silicates. Turbulent mixing transports the annealed silicate dust beyond the disk zone, where it has been formed, and replaces part of the amorphous silicate in the outer regions of the disk. In Paper I the impact of annealing on the global structure of disks already has been

studied within the frame of stationary models, particular its effect on the temperature at the disk's midplane.

Figure 1 sketches a possible sequence of events for annealing of a dust particle. Initially the grain exhibits small areas of crystalline structure within the amorphous texture of the grain, at least for pure statistical reasons. These areas act as seeds for the further crystallisation. At sufficiently high temperature the SiO_4 tetrahedrons are excited to a sufficiently high kinetic energy to surmount the energy barriers, which previously inhibited them from accessing energetically more favourable positions and orientations in the lattice. If we ignore domain boundaries, the grain finally will be completely crystallised. In this scenario the process of crystallisation, of course, also can cease if the temperature drops untimely, leeding to partially crystallised grain (middle image in Fig. 1).

By assuming spherical growth of the small crystalline seeds the increment of volume of a single crystallised domain $V_{\rm cry}$ is approximately (Gail 1998)[1]

$$\frac{{\rm d}V_{\rm cry}}{{\rm d}t} = 6V_{0,\rm sil}^{\frac{1}{3}} V_{\rm cry}^{\frac{2}{3}} \nu_{\rm vib} {\rm e}^{-E_{\rm a}/k_{\rm B}T_{\rm c}}, \tag{5}$$

where $V_{\rm cry}$ is the volume of crystallised silicate within the grain, $V_{0,\rm sil}$ the volume of a SiO_4 tetrahedron (calculated as in Eq. (2)), $\nu_{\rm vib}$ the characteristic frequency of lattice vibrations and $E_{\rm a}$ the activation energy for rearrangement processes in the lattice due to annealing, respectively. We use laboratory data from recent annealing experiments of Fabian et al. (2000) who found $E_{\rm a}/k_{\rm B} = 39\,100 \pm 400\,{\rm K}$ for the annealing of forsterite and employ $\nu_{\rm vib} = 2 \times 10^{13}\,{\rm s}^{-1}$ (Lenzuni et al. 1995; Duschl et al. 1996). In our model calculations we consider forsterite (Mg_2SiO_4) as the only silicate dust component, since it is the most abundant silicate in protoplanetary disks. Enstatite ($MgSiO_3$) and quartz (SiO_2) are not considered.

In Eq. (5) we do not take into account that separate crystallised areas overlap in the late phase of annealing, as it is shown in Fig. 1. However, this seems to have an only slight effect on the results of the models, since, if overlapping becomes important, annealing of grains has already progressed to a large extent.

Using $V_{\rm cry}$ from Eq. (5), the degree of crystallisation of the grain is determined by

$$x_{\rm cry} = \min\left(\frac{n_{\rm cry} V_{\rm cry}}{V_{0,\rm sil}}, 1\right), \tag{6}$$

where $n_{\rm cry}$ is the fraction of growth centers per silicon atom, i.e. the fraction of nucleation seeds. With Eqs. (5) and (6), by introducing a discrete set x_i $(i = 1 \ldots M)$ of degrees of crystallisation $x_{\rm cry}$, we obtain the characteristic time of annealing for a forsterite grain with degree of crystallisation $x_{i,\rm cry}$ into a forsterite grain with degree of crystallisation $x_{i+1,\rm cry}$ (Paper I)

$$\tau_{i,i+1,\rm for} = \frac{x_{i+1,\rm cry}^{1/3} - x_{i,\rm cry}^{1/3}}{2\nu_{\rm vib} n_{\rm cry}^{1/3}} {\rm e}^{E_{\rm a}/k_{\rm B}T_{\rm c}}. \tag{7}$$

In our model calculations we set $n_{\rm cry} = 10^{-5}$. Due to the weak dependency of the characteristic time of annealing (7) on $n_{\rm cry}$ the choice of $n_{\rm cry}$ has not too much effect on the results for the disk structure[2].

2.3. The diffusion-transport-reaction equation

Obviously in accretion disks there operates a process which forces them to transport their matter inside (finally onto the central object) and their angular momentum outside. In our model calculations for protoplanetary disks we assume that this process is due to turbulent motions as a result of convection, since the disks are convectively unstable in the vertical direction during their lifetime over a wide spatial range (Lin & Papaloizou 1980; Ruden & Lin 1986; D'Alessio et al. 1998). Additional to or instead of convection, there may operate other sources of turbulence in protoplanetary disks, e.g. shearing (Dubrulle 1993), a baroclinic instability (Cabot 1984) and a magnetic instability (Balbus & Hawley 1991). We conclude that the turbulent flow induces a diffusion like mixing of the matter in the disk, which consists of a gas-dust mélange.

Because of the low particle density of the dust and gas species in protoplanetary disks, except for hydrogen and helium, the different tracers can be treated independently of each other. In the one zone approximation the diffusion-transport-reaction equation of a tracer, embedded in a carrier gas of much higher particle density, is (e.g. Hirschfelder et al. 1964; Paper I)

$$\frac{\partial c_{i,j}}{\partial t} + v_r \frac{\partial c_{i,j}}{\partial r} = \frac{1}{rn}\frac{\partial}{\partial r} rn D_{\rm dg} \frac{\partial c_{i,j}}{\partial r} + \frac{c_{i-1,j}}{\tau_{i-1,i,j}} - \frac{c_{i,j}}{\tau_{i,i+1,j}}. \tag{8}$$

The second term on the l.h.s. is the advection term, the first one on the rhs the diffusion term and the following terms on the rhs the gain and loss terms. In Eq. (8) $c_{i,j}$ is the concentration of the species j (in our case carbon and forsterite), which occur in different properties i (in our case carbon grains of different radii and forsterite grains of different degrees of crystallisation), r is the radial distance from the protostar, v_r the radial component of the tracer's velocity, n the total particle density (mainly due to H_2 and He) and $D_{\rm dg}$ the binary diffusion coefficient of a dust tracer of low density in the carrier gas, respectively. The characteristic timescales $\tau_{i,i+1,j}$ are given by Eqs. (4) and (7), respectively.

[1] Desintegration of the solid into microcrystalline areas with different chemical composition and exsolution of existent impurities is not considered here.

[2] However, for the smallest silicate grains with a diameter $a \lesssim 10\,{\rm nm}$ our assumptions fail, since these grains hold less than 10^5 silicon atoms and thus most of them contain no nucleation seed for annealing.

The binary diffusion coefficient is related to the viscosity ν of the disk matter by

$$D_{\rm dg} = \frac{\nu}{S_{\rm dg}}, \tag{9}$$

where $S_{\rm dg}$ is the Schmidt number for the dust species in the carrier gas. In Eq. (9) we assume that it makes no difference whether the dust particles are transported by random thermal motions (where the original definition of the Schmidt number comes from; Waldmann 1958) or – as in our case – by turbulence. The Schmidt number provides information about the strength of frictional coupling between the dust particles and the carrier gas. If $S_{\rm dg}^{-1}$ (an inverse Prandtl number) is unity, the velocity of the dust particles relative to the carrier gas vanishes, i.e the particles move around as the gas. In contrast, if $S_{\rm dg}^{-1}$ vanishes, the dust particles moves independent of the carrier gas, i.e. frictional forces due to the gas have no influence on the motion of the particles. The value of $S_{\rm dg}^{-1}$ mainly depends on the size of the dust particles and the density of the carrier gas. In protoplanetary disks the dust particles are strongly coupled to the gas up to roughly mm size across a wide spatial range (Weidenschilling & Cuzzi 1993). The present model calculations of protoplanetary disks consider dust particles with a maximum size of about $1\,\mu$m and do not include dust coagulation. Therefore we approximate[3]

$$S_{\rm dg} = 1. \tag{10}$$

Laboratory experiments with small sized particles in flow systems also yield Schmidt numbers of roughly unity (Launder 1976; McComb 1990).

In the present model infall of matter from the ambient molecular cloud onto the disk is neglected. In case of infall a source term for the infalling matter has to be added on the r.h.s. of Eq. (8). Model calculations with infall of matter will be the subject of future investigations.

The quantities $n_{\rm OH}$, $T_{\rm c}$, v_r, n and ν in Eqs. (4), (7), (8) and (9), respectively, will be calculated from the equations for the radial disk structure in the one-zone approximation (see Sect. 3.1). In the following the binary diffusion coefficient (9) is denoted by D.

2.4. Solution of the diffusion-transport-reaction equation

The calculation of the carbon combustion and the annealing of silicate dust in our numerical model of protoplanetary accretion disks requires the solution of the set of diffusion-transport-reaction Eqs. (8). For this purpose we define a logarithmic grid for the carbon grain size a_i ($i = 1 \ldots N$, $N = 31$) with $a_1 = 0.25\,\mu$m and $a_N = 0.001\,\mu$m and an equidistant grid for the degree of crystallisation of the silicate grains $x_{i,\rm cry}$ ($i = 1 \ldots M$, $M = 11$) with $x_{1,\rm cry} = 0.0$, $x_{2,\rm cry} = 0.1$, $x_{3,\rm cry} = 0.2$, …, $x_{M,\rm cry} = 1.0$. The choice of the size distribution of carbon grains is motivated by the choice for the initial boundary conditions for the $c_{i,j}$ which is a MRN size distribution (see Sect. 4.1).

For the purpose of numerical calculations the set of diffusion-transport-reaction Eqs. (8) is replaced by the set of difference equations

$$\begin{aligned}
\frac{c_{i,j,k}^{n+1} - c_{i,j,k}^{n}}{\Delta t} = (1-\Theta) \Bigg[& \frac{(rnD)_{k+\frac{1}{2}}^{n+1} (c_{i,j,k+1}^{n+1} - c_{i,j,k}^{n+1})}{n_k^{n+1} r_k h_{{\rm m},k} h_{{\rm r},k}} \\
& - \frac{(rnD)_{k-\frac{1}{2}}^{n+1} (c_{i,j,k}^{n+1} - c_{i,j,k-1}^{n+1})}{n_k^{n+1} r_k h_{{\rm l},k} h_{{\rm m},k}} \\
& + \frac{c_{i-1,j,k}^{n+1}}{\tau_{i-1,i,j,k}^{n+1}} - \frac{c_{i,j,k}^{n+1}}{\tau_{i,i+1,j,k}^{n+1}} - a_{i,j,k}^{n+1} \Bigg] \\
+ \Theta \Bigg[& \frac{(rnD)_{k+\frac{1}{2}}^{n} (c_{i,j,k+1}^{n} - c_{i,j,k}^{n})}{n_k^{n} r_k h_{{\rm m},k} h_{{\rm r},k}} \\
& - \frac{(rnD)_{k-\frac{1}{2}}^{n} (c_{i,j,k}^{n} - c_{i,j,k-1}^{n})}{n_k^{n} r_k h_{{\rm l},k} h_{{\rm m},k}} \\
& + \frac{c_{i-1,j,k}^{n}}{\tau_{i-1,i,j,k}^{n}} - \frac{c_{i,j,k}^{n}}{\tau_{i,i+1,j,k}^{n}} - a_{i,j,k}^{n} \Bigg],
\end{aligned} \tag{11}$$

where we have introduced the abbreviations

$$\begin{aligned}
h_{{\rm l},k} &= r_k - r_{k-1} \\
h_{{\rm m},k} &= \frac{1}{2}\,(r_{k+1} - r_{k-1}) \\
h_{{\rm r},k} &= r_{k+1} - r_k,
\end{aligned} \tag{12}$$

$$\begin{aligned}
(rnD)_{k+\frac{1}{2}}^{n} &= \frac{1}{2}\left(r_{k+1} n_{k+1}^{n} D_{k+1}^{n} + r_k n_k^{n} D_k^{n}\right) \\
(rnD)_{k-\frac{1}{2}}^{n} &= \frac{1}{2}\left(r_k n_k^{n} D_k^{n} + r_{k-1} n_{k-1}^{n} D_{k-1}^{n}\right)
\end{aligned} \tag{13}$$

and

$$a_{i,j,k}^{n} = \begin{cases} v_{r,k}^{n} \dfrac{c_{i,j,k+1}^{n} - c_{i,j,k}^{n}}{h_{{\rm r},k}} & v_{r,k}^{n} \le 0 \\ v_{r,k}^{n} \dfrac{c_{i,j,k}^{n} - c_{i,j,k-1}^{n}}{h_{{\rm l},k}} & v_{r,k}^{n} > 0, \end{cases} \tag{14}$$

respectively. The index k denotes the grid-point at the radial distance r_k, the index n the grid-point of the time grid t_n and $\Delta t = t_{n+1} - t_n$ the current time step. The advection term (14) is treated by a simple upwind method.

The set of Eqs. (11) is solved by standard methods (fully implicit, i.e. $\Theta = 0$), starting from the equation with $i = 1$ (largest carbon grains, completely amorphous silicate grains) and successively continuing with the equations with $i = 2, 3, \ldots$ up to N or M, for carbon combustion or annealing, respectively. It is an important simplification for the solution of the set of Eq. (11) that the equation i exclusively couples with the next equation $i + 1$, i.e. it is assumed that carbon grains do not grow in size (due to condensation or coagulation) and that partially or completely annealed silicate grains do not become

[3] Strictly speaking, this approximation fails in the outer zones of the disk, where the gas density becomes low.

amorphous again (supported by the fact that no physical process is known, which could do this in protoplanetary disks).

Note that for the rate terms in Eqs. (11) and (8) some of the terms have to be omitted at the boundaries of the i-grids:

In the case $i = 1$ there exists no gain term, since $(i, j) = (1, \mathrm{car})$ refers to the carbon grains with maximum size in our model calculations and $(i, j) = (1, \mathrm{for})$ refers to forsterite grains with a degree of crystallisation of zero, respectively. For $i = 1$ only the loss terms have to be considered.

In the case $(i, j) = (M, \mathrm{for})$ no losses occur, since the forsterite grains are already completely annealed. The corresponding terms have to be omitted in this case.

In the case $(i, j) = (N, \mathrm{car})$, losses correspond to the complete combustion of carbon grains, thus Eq. (11) is correct at $(i, j) = (N, \mathrm{car})$.

The choice of boundary conditions, which are required for solving the set of diffusion-transport-reaction Eqs. (8), will be discussed in Sect. 4.

3. The global structure and evolution of the disk

This section presents the equations for our model of the radial structure and temporal evolution of protoplanetary disks.

The present model calculations are performed in the one-zone approximation, therefore all disk quantities are evaluated at (or close to) the disk midplane. The sole heating mechanism of the disk is assumed to be viscous dissipation. This assumption is supported by the vertical disk models of D'Alessio et al. (1998), who found stellar irradiation to be the most important heating source of the disk atmosphere, but viscous dissipation dominating for the heating close to the disk midplane.

Gas and dust are supposed to be in thermal equilibrium. The condensation of the main dust absorbers (except for solid carbon) is calculated for an equilibrium state, and we take care of an as accurate as possible specification of the opacity of the disk matter. Coagulation of dust or formation of larger bodies are not considered.

3.1. The disk equations

We assume geometrically thin viscous Keplerian α-disks in the one zone approximation. From the equation of angular momentum conservation one derives the equation

$$\frac{\partial \Sigma}{\partial t} = \frac{3}{r}\frac{\partial}{\partial r}\sqrt{r}\frac{\partial}{\partial r}\nu\Sigma\sqrt{r} \tag{15}$$

for the global evolution of the surface density Σ (e.g. Pringle 1981). ν is the viscosity.

Equation (15) is a differential equation of diffusion type, as the diffusion-transport-reaction Eq. (8), but without the advection and rate terms. Thus it can easier be solved than (8) (again fully implicitly).

While the accretion disk evolves it loses matter through its inner boundary. Using their numerical model for protoplanetary accretion disks Ruden & Pollack (1991) pointed out that the mass loss onto the star amounts to about one half of the initial disk mass for the first million years of disk evolution. Thus accretion of mass onto the star has to be taken into account. The (time dependent) disk mass is given by

$$M_{\mathrm{disk}}(t) = \int_{r_\mathrm{i}}^{r_\mathrm{o}} 2\pi r \Sigma(r, t)\,\mathrm{d}r. \tag{16}$$

r_i and r_o are the inner and outer boundaries of the disk, respectively. Consequently for the (time dependent) stellar mass one has

$$M_*(t) = M_{*,0} + M_{\mathrm{disk},0} - M_{\mathrm{disk}}(t). \tag{17}$$

$M_{*,0}$ and $M_{\mathrm{disk},0}$ are the initial stellar and disk masses, respectively. Equation (17) holds if the outer boundary r_o is chosen to be large enough such that the outward directed radial mass transport of matter does not lead to significant mass loss through r_o in late phases of the disk evolution. Again, we do not consider infall of matter onto the disk.

Besides Eq. (15) for the evolution of the surface density Σ we need equations for calculating the radial structure of the disk. In case of a thin Keplerian α-disk in the one-zone approximation the basic set of equations is (Pringle 1981; Lin & Papaloizou 1985; Ruden & Pollak 1991):

1.) The Keplerian angular velocity of matter in the disk:

$$\Omega = \sqrt{\frac{GM_*}{r^3}}. \tag{18}$$

G is the gravitational constant and M_* the mass of the protostar. We do not consider self gravitation of the disk, as well as we do not consider the influence of the radial pressure gradient on the motion of the disk matter around the central star.

2.) The isothermal sound speed:

$$c_\mathrm{s} = \sqrt{\frac{k_\mathrm{B}T_\mathrm{c}}{\mu m_\mathrm{H}}}. \tag{19}$$

μ is the mean molecular weight of the disk matter.

3.) The pressure scale height, calculated at the midplane of the disk:

$$h_\mathrm{s} = \frac{c_\mathrm{s}}{\Omega}. \tag{20}$$

4.) The viscosity in the α-approximation of Shakura & Sunyaev (1973):

$$\nu = \alpha\, h_\mathrm{s} c_\mathrm{s}. \tag{21}$$

α is the parameter of the efficiency of turbulent viscosity. This is also the viscosity ν used for evaluating the diffusion coefficient (9).

5.) The effective temperature of the disk surface:

$$\sigma T_{\rm eff}^4 = \frac{9}{8}\Omega^2 \nu\Sigma + \sigma T_{\rm cloud}^4. \tag{22}$$

σ is the Stefan-Boltzmann constant and $T_{\rm cloud}$ the temperature of the ambient molecular cloud. In the derivation of Eq. (22) it is assumed that dissipation of kinetic energy through viscous processes is the sole energy source. The energy production is limited to the disk midplane. The energy transport occurs exclusively in the vertical direction and by radiation in an approximately plane parallel, geometrically thin disk.
6.) The mean vertical mass density:

$$\rho_{\rm m} = \frac{\Sigma}{2h_{\rm s}}. \tag{23}$$

Note that $\rho_{\rm m}$ is not the central mass density but is lower than this by a factor of roughly 2.
7.) The mean molecular weight:

$$\mu = \mu(\rho_{\rm m}, T_{\rm c}). \tag{24}$$

The mean molecular weight (24) in principle is a function of temperature and mass density. We use a fixed value of $\mu = \frac{7}{3}$ valid for a mixture of molecular hydrogen and helium with a helium abundance of 0.1 relative to H. In our models the disk is hot enough for dissociation of H_2 only close to the inner boundary and solely in early evolutionary stages. The degree of dissociation of H_2 has no significant effect on the behaviour of the dust, hence dissociation of H_2 is neglected. Note that in Paper I dissociation of H_2 was considered.
8.) The Rosseland mean of the mass extinction coefficient of the disk matter at the midplane:

$$\kappa_{\rm R} = \kappa_{\rm R}(\rho_{\rm m}, T_{\rm c}). \tag{25}$$

The opacity (25) is a function of temperature and mass density. The way of its calculation will be discussed in the following subsection.
9.) The vertical optical depth at the midplane:

$$\tau_{\rm c} = \frac{1}{2}\Sigma\kappa_{\rm R}. \tag{26}$$

Equation (26) only holds for a constant opacity. In the case of a slight dependence of the opacity on temperature and density, as in our case, Eq. (26) at least is an acceptable approximation.
10.) The temperature at the midplane:

$$T_{\rm c}^4 = T_{\rm eff}^4\left(\frac{1}{2} + \frac{3}{4}\tau_{\rm c}\right) + T_{\rm cloud}^4. \tag{27}$$

Equation (27) is the vertical temperature stratification in the Eddington approximation according to the theory of plane parallel stellar atmospheres. The last term at the r.h.s. is added to account for the disk irradiation by the molecular cloud which at the same time ensures $T_{\rm c} \geq T_{\rm cloud}$ for the cool parts of the disk far away from the central star. For the chemical active zone of the disk this term is negligible.

Equations (18)–(27) represent the basic set of equations for the radial structure of the disk. It is solved by iterating $T_{\rm c}$ up to an accuracy of 10^{-7}. Additionally there are some other important variables.
11.) The pressure close to the midplane:

$$P_{\rm c} = c_{\rm s}^2\,\rho_{\rm m}. \tag{28}$$

12.) The total particle density close to the midplane:

$$n = \frac{P_{\rm c}}{k_{\rm B}T_{\rm c}}. \tag{29}$$

13.) The pressure of OH molecules close to the midplane:

$$p_{\rm OH} = p_{\rm O}p_{\rm H}K_p({\rm OH}). \tag{30}$$

$p_{\rm O}$ and $p_{\rm H}$ are the partial pressures of free oxygen and hydrogen atoms, respectively, and K_p(OH) is the constant of the law of mass action for the OH molecule. The calculation of $p_{\rm O}$ and $p_{\rm H}$ is described in Paper I. In Eq. (30) we assume that the loss of OH molecules due to carbon combustion is counterbalanced by the gain of OH molecules due to its production by H_2 dissociation and the reaction $H + H_2O \rightarrow OH + H_2$ of the free H atoms. In principle one has to solve an extended chemical reaction network which, however, is out of the scope of the present work.
14.) The mass accretion rate:

$$\dot{M} = -6\pi\sqrt{r}\,\frac{\partial}{\partial r}\nu\Sigma\sqrt{r}. \tag{31}$$

15.) The radial drift velocity:

$$v_r = \frac{\dot{M}}{2\pi r\Sigma}. \tag{32}$$

The radial drift velocity determines the advection term (14) for calculating the set of diffusion-transport-reaction Eqs. (11).

3.2. The opacity

In this work a main focus is centered on an accurate treatment of the disks opacity. The opacity (25) essentially is calculated as in Paper I, however, some modifications are required for the present model calculation.

The Rosseland mean of the opacity of the gas-dust mixture is approximated by

$$\kappa_{\rm R} = \kappa_{\rm gas} + f_{\rm ice}\kappa_{\rm R,ice} + (1 - f_{\rm ice})\sum_j f_j\kappa_{{\rm R},j}. \tag{33}$$

$\kappa_{\rm gas}$ is the opacity of the disk gas and $\kappa_{{\rm R},j}$ the Rosseland mean of the opacity of each dust species j and f_j its degree of condensation[4]. The dust species which we have to

[4] $\kappa_{{\rm R},j}$ corresponds to the opacity of species j if the key element required for its formation (e.g. Si for silicates, C for carbon dust) is completely condensed into this dust species. Then $f_j\kappa_{{\rm R},j}$ is the opacity in case of an only partial condensation of the key element into the dust species.

consider are ice coated grains, silicate grains (forsterite), carbon grains, iron grains and corundum grains. These are supposed to be the most important absorbers. We just add up the Rosseland means of the different dust species, i.e. we assume an essentially grey extinction. The factors $f_{\rm ice}$ and $(1-f_{\rm ice})$ in Eq. (33) serve for a smooth transition of $\kappa_{\rm R}$ in the zone of ice vaporization.

The condensation degrees f_j (specified: $f_{\rm ice}$, $f_{\rm for}$, $f_{\rm car}$, $f_{\rm iro}$ and $f_{\rm cor}$, respectively) are calculated as in Paper I. The degree of condensation of ice for ice coated grains is given by

$$f_{\rm ice} = \max\left(1 - \frac{p_{\rm v,ice}}{p_{\rm H_2O}}, 0\right), \tag{34}$$

where $p_{\rm v,ice}$ is the vapour pressure of ice, calculated from an approximation formula of Lichtenegger & Kömle (1991). The steam pressure $p_{\rm H_2O}$ is calculated as in Paper I.

The degree of condensation of carbon is given by

$$f_{\rm car} = \frac{1}{V_{0,\rm car}\epsilon_{\rm C}} \sum_{i=1}^{N} \frac{4\pi}{3} a_i^3 c_{i,\rm car}. \tag{35}$$

$\epsilon_{\rm C}$ is the abundance of carbon nuclei with respect to hydrogen nuclei. For the mixture of amorphous and crystalline silicate grains the opacity is approximated by

$$\kappa_{\rm R,sil} = f_{\rm cry,for}\kappa_{\rm R,sil,cry} + (1-f_{\rm cry,for})\kappa_{\rm R,sil,am}, \tag{36}$$

where the indices "cry" and "am" mean crystalline and amorphous. $f_{\rm cry,for}$ is the average degree of crystallised silicate which is given by

$$f_{\rm cry,for} = \sum_{i=1}^{M} x_{i,\rm cry} c_{i,\rm for}. \tag{37}$$

The concentrations $c_{i,j}$ in Eqs. (35) and (37) follow from the solution of the diffusion-transport-reaction Eq. (8).

For $\kappa_{\rm R,sil,cry}$ we use data for the optical constants of crystalline olivine (Huffman, private communication), in case of $\kappa_{\rm R,sil,am}$ data of amorphous forsterite (Draine & Lee 1984; Draine 1985). For calculating the degree of condensation of silicate grains $f_{\rm for}$ only forsterite is considered. This is a slight simplification in order to hold the number of dust species as low as possible. Optical data for the other dust species are taken from Lide (1995) (in case of iron), Koike et al. (1995) (corundum) and Draine & Lee (1984), Draine (1985) (carbon). The Rosseland mean of the opacities of each dust species are calculated by Mie theory and assuming a Mathis-Rumpl-Nordsieck (MRN) size distribution for each species (Mathis et al. 1977). For the opacity of ice coated grains $\kappa_{\rm R,ice}$ we use the approximation of Bell & Lin (1994).

In the special case of carbon dust the grain size distribution changes with time due to carbon combustion. But, anticipating a result of our model calculations, the grain size distribution of carbon does not deviate far from the initial MRN distribution. Thus we compute the Rosseland mean of carbon dust by using the MRN size distribution throughout the entire evolution of the disk.

The opacity of the gas $\kappa_{\rm gas}$ is calculated by

$$\kappa_{\rm gas} = \left(\frac{1}{\kappa_{\rm mol}^4} + \frac{1}{\kappa_{\rm at}^4 + \kappa_{\rm el}^4}\right)^{-\frac{1}{4}}. \tag{38}$$

$\kappa_{\rm mol}$, $\kappa_{\rm at}$ and $\kappa_{\rm el}$ are the opacities of molecules, atoms/ions and free electrons, respectively, calculated with the approximations of Bell & Lin (1994). The special kind of interpolation in Eq. (38) defines smooth transition zones between the opacity regimes. The opacity of H^- is omitted to avoid thermal instabilities due to the steep temperature dependent rise of the opacity in the region of the existence of negative hydrogen ions (Bell & Lin 1994; Hartmann & Kenyon 1996). This approximation has little effect to our model since we are particularly interested in the physical and chemical conditions within disk regions with an only moderately high temperature where dust exists, and disregard the extreme processes appearing within the hot inner part of the disk. In case of models for cool disks H^- absorption does not play any role anyway.

4. Numerical proceeding

This section presents the choice for the boundary conditions and model parameters and the method of calculating of the numerical model.

4.1. Initial and boundary conditions

The solution of the set of diffusion-transport-reaction Eqs. (8) and the equation for the evolution of the surface density (15) requires the prescription of initial and boundary conditions.

4.1.1. Initial conditions

In case of the initial conditions, Σ and $c_{i,j}$ have to be specified for each (i,j) at each of the radial grid points. The solutions of Eqs. (8) and (15) have the property to develop to asymptotic terminal states due to their diffusion like type, in which the inner part of the disk evolves through a series of quasi-stationary states, while the outer parts expand in time. For our purposes a relaxation towards these terminal states is desired as fast as possible since we are interested in physical and chemical conditions in the disk at an evolution time as early as possible. Hence, we wish to start with initial models which are already close to the asymptotical states which develop after an initial transient period. For this purpose we choose stationary disk models as initial condition.

More precisely, we choose stationary disk models constructed by the methods of Paper I including the calculation of carbon combustion but by suppressing the calculation of silicate annealing. This guarantees an appropriate initial specification of Σ, $c_{i,\rm car}$ and $c_{i,\rm cr}$ for every i at

Table 1. Parameters used for the calculation of the disk models.

initial stellar mass	$M_{*,0}$	1 $M_\odot$
stellar effective temperature	T_*	4500 K
stellar luminosity	L_*	5 $L_\odot$
stellar radius	R_*	3.688 $R_\odot$
inner disk radius	r_i	5 R_*
outer disk radius	r_o	200 AU
molecular cloud temperature	T_cloud	20 K
initial disk mass	$M_\mathrm{disk,0}$	0.2 $M_\odot$
disk angular momentum	J_disk	10^{53} g cm^2 s^{-1}
viscosity parameter	α	10^{-3}, 3×10^{-3}, 10^{-2}

each radial grid point. The suppression of silicate annealing means that initially there is no crystallised silicate in the disk. This should be a good assumption as there is little or even no crystallised silicate in the interstellar medium.

For carbon dust grains the initial size distribution is assumed to be given by the MRN size distribution (Mathis et al. 1977). Due to the weakness of the accretion shock for mass-infall onto the outer parts of the disk dust grains survive almost unmodified, and their size distribution should be that of interstellar dust grains, which we assume to be given by the widely used MRN size distribution[5]. The initial value for the degree of condensation of carbon is set to $f_{0,\mathrm{car}} = 0.6$ (Mathis et al. 1977), as in Paper I. The remaining carbon is assumed to be bound in CO.

4.1.2. Boundary conditions

The boundary conditions for the concentration $c_{i,j,k}$ at the inner and outer borders of the radial grid are determined as follows: at the inner boundary the silicate is completely annealed and the carbon dust completely burnt (cf. Eqs. (19) and (35) of Paper I). At the outer boundary the silicate dust is completely amorphous and the size distribution of carbon dust, again, equals the MRN distribution as initially assumed to be valid for the dust from the molecular cloud (cf. Eqs. (22) and (36) of Paper I).

The surface density Σ is assumed to vanish both at the inner and outer boundary. At the outer boundary this choice is reasonable since the surface density becomes extremely low far away from the protostar. At the inner boundary this choice seems to be unreasonable since the surface density usually rises with decreasing radial distance to the star. However, this choice is common practise in evolutionary calculations of one-zone models because it has two advantages. At one hand the solution of Eq. (15) becomes much easier as in the case of non-vanishing boundary condition. On the other hand this choice ensures that the matter which passes through the inner boundary is definitely extracted from the disk and falls onto the protostar. As a result of this choice for the inner boundary condition the surface density decreases unphysically close to the inner boundary. However, we found in our model calculations that this has no significant influence on the disk structure in those regions of the disk where dust does exists.

[5] Different size distribution of ISM dust grains have been proposed by Weingartner & Draine (2001).

Table 2. Parameters for the initial mass accretion rate at the edges of the disk (in units of 10^{-9} $M_\odot\,\mathrm{yr}^{-1}$; cf. Eq. (43)) for our different models, and angular momenta of disks with given viscosity parameters α calculated from Eq. (39) of Stepinski (1998) and Eq. (40) of Nakamoto & Nakagawa (1995) in units of 10^{53} g cm^2 s^{-1}. In the present model calculations the angular momentum J_disk of the disk is set to 10^{53} g cm^2 s^{-1} in each model.

model	α	$\dot{M}_\mathrm{a}$	$\dot{M}_\mathrm{b}$	$J_\mathrm{disk,ste}$	$J_\mathrm{disk,nak}$
a1	1×10^{-3}	95.000	2.8126	0.640	0.646
a3	3×10^{-3}	364.78	8.1997	0.930	0.784
a10	1×10^{-2}	1714.6	26.963	1.400	1.002

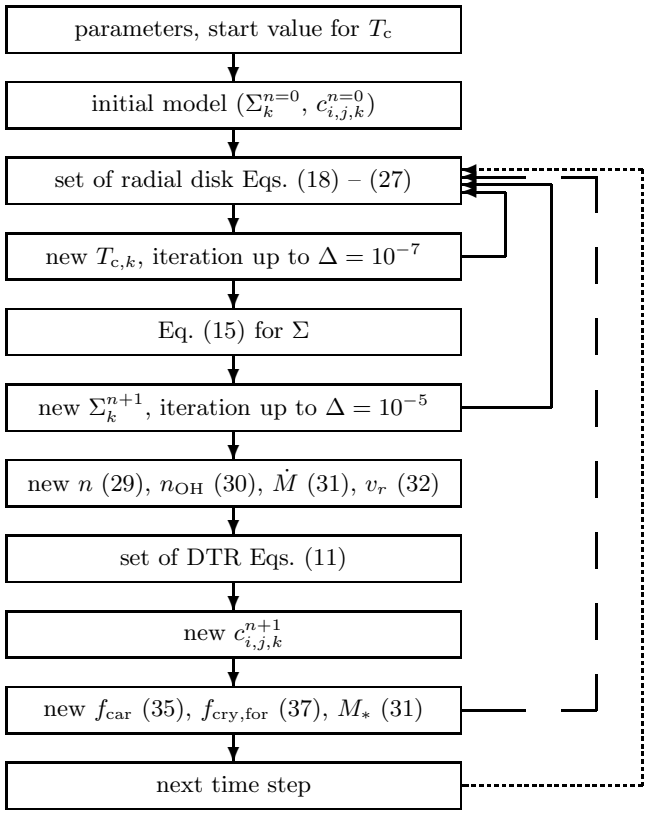

Fig. 2. Flow chart of the numerical code (for details see text). Δ denotes the accuracy of the iteration, and the term "diffusion-transport-reaction" is abbreviated by DTR. Arrows with full lines denote iteration steps. The arrow with dashed lines marks the iteration of the concentrations $c_{i,j,k}^{n+1}$, which is omitted in our model calculations, and the arrow with dotted lines denotes the loop.

4.2. Model parameters

Next we have to choose a set of parameters for the disk model. With respect to the properties of observable star-disk systems in a quiescent state (e.g. Natta 2000) we determine a set of parameters typically for protostars and protoplanetary disks (Table 1).

With respect to the viscosity parameter α and the angular momentum $J_{\rm disk}$ of the disk Stepinski (1998) and Nakamoto & Nakagawa (1995) derived quite similar relations between these quantities. Stepinski (1998) compared disk observations with a big number of simple semi-analytic disk models and found the relation

$$J_{\rm disk,ste} \approx 6.7\alpha^{0.34} \tag{39}$$

for stars with masses of $0.85{-}1.62\,M_\odot$, where $J_{\rm disk,ste}$ is in units of $10^{53}\,{\rm g\,cm^2\,s^{-1}}$. Nakamoto & Nakagawa (1995) calculated numerical models for the growth of protoplanetary disks and obtained

$$\log J_{\rm disk,nak} = 0.577 - \sqrt{-0.256\log\alpha - 0.180} \tag{40}$$

for a final disk-to-star mass ratio $M_{\rm disk}/M_{\rm ast}$ of about 0.1 after 10^6 yr. According to Ruden & Pollack (1991) the initial disk-to-star mass ratio exceeds the final value by a factor of about 2. $J_{\rm disk,nak}$ also is in units of $10^{53}\,{\rm g\,cm^2\,s^{-1}}$. Calculated and observed lifetimes of α-disks agree reasonably well for a choice of α between 10^{-2} and at least 10^{-3} (Ruden & Pollack 1991; Calvet et al. 2000; Drouart et al. 1999). The proper range of angular momenta $J_{\rm disk}$ for these values of α according to (39) and (40) are shown in Table 1. A reasonable choice of $J_{\rm disk}$ then is to set the disk's angular momentum $J_{\rm disk}$ to $10^{53}\,{\rm g\,cm^2\,s^{-1}}$ for each of our models with different viscosity parameters α.

The initial disk mass $M_{\rm disk,0}$ is chosen to be below the reference point of Shu et al. (1990) for disk stability against gravitational perturbations. The stellar radius follows from the relation

$$L_* = 4\pi R_*^2\,\sigma T_*^4. \tag{41}$$

The initial disk mass $M_{\rm disk,0}$ and the angular momentum of the disk

$$J_{\rm disk} = \int_{r_{\rm i}}^{r_{\rm o}} 2\pi r^3 \Omega\Sigma\,{\rm d}r \tag{42}$$

are determined by the mass accretion rate $\dot M$ of the initial stationary model.

To get simultaneously the adopted values for the initial disk mass $M_{\rm disk,0}$ and angular momentum $J_{\rm disk}$, $\dot M$ generally can not be constant, as it is assumed in the stationary models of Paper I, but has to be assumed as radially dependent in a suitable fashion. We specify a fermi-like distribution as initial distribution for the radial dependence of the accretion rate

$$\dot M(r) = \begin{cases} \dot M_{\rm a} & \text{at} \quad r < r_{\rm a} \\ \dot M_{\rm a}\left(\dfrac{\dot M_{\rm b}}{\dot M_{\rm a}}\right)^{\frac{r_{\rm a}^2 - r^2}{r_{\rm a}^2 - r_{\rm b}^2}} & \text{at} \quad r_{\rm a} < r < r_{\rm b} \\ \dot M_{\rm b} & \text{at} \quad r > r_{\rm b}, \end{cases} \tag{43}$$

where $\dot M_{\rm a}$ and $\dot M_{\rm b}$ are the mass accretion rates at the borders of the variable part of the radial $\dot M$-distribution between $r_{\rm a} = 5\,{\rm AU}$ and $r_{\rm b} = 50\,{\rm AU}$, respectively. This choice of $\dot M(r)$ is somewhat arbitrary, but in our numerical model calculations after an initial transient time the local accretion rate $\dot M$ calculated according to (31) is independent of the particular choice of the initial model. In this work we study models with three different values for the viscosity parameters, $\alpha = 10^{-3}$, 3×10^{-3} and 10^{-2}, which in the following are abbreviated as a1, a3 and a10. The values of $\dot M_{\rm a}$ and $\dot M_{\rm b}$ for the different initial models are shown in Table 2. The resulting initial $\dot M(r)$ from model a3 is shown as an example in the upper part of Fig. 4.

4.3. Numerical treatment of the model

The numerical method of the present model calculation is as follows (cf. Fig. 2):

Within a given time step, Eq. (15) for the surface density is solved using standard methods for parabolic equations. The value of ν that is required for the solution of Eq. (15) is calculated by solving the set of equations for the radial disk structure (18)–(27) since ν itself depends on Σ. This requires an iteration of Σ and $\nu(\Sigma)$ for self consistency which is done by a fixpoint iteration up to an accuracy of 10^{-5} for Σ.

The set of radial disk Eqs. (18)–(27) is solved by first assuming a value of $T_{\rm c}$ and going stepwise through Eqs. (18)–(27) until we obtain from (27) a new value for $T_{\rm c}$. Then $T_{\rm c}$ is iterated with a bisection method up to an accuracy of 10^{-7}.

Then the set of diffusion-transport-reaction Eqs. (11) is solved with standard methods, using the values of v_r, n, ν, $T_{\rm c}$ and $n_{\rm OH}$ from the solution of the set of equations for the radial disk structure (18)–(30) from the last iteration step for Σ. The resulting concentrations $c_{i,j,k}$ determine the degree of crystallisation of forsterite grains $f_{\rm cry,for}$ and the degree of condensation of carbon grains $f_{\rm car}$ by Eqs. (37) and (35). The values of $c_{i,j,k}$, $f_{\rm cry,for}$ and $f_{\rm car}$ then are used for the next time step.

Finally the stellar mass M_* is re-calculated from Eqs. (16) and (17), and the next time step is performed.

The global numerical method of the model calculation is not fully implicit. It contains an explicit part, since the concentrations $c_{i,j,k}$ are not iterated for the new time step. There is an additional explicit part with respect to the stellar mass for which we always use the value from the last time step, because the mass accretion onto the star is a slow process. We did a test calculation for model a3 with a fixpoint iteration for $c_{i,j,k}$ by using the new values of $c_{i,j,k}$ for re-calculating Σ and $\nu(\Sigma)$ at the new time step and iterating up to an accuracy of 10^{-5}. This iteration is indicated in Fig. 2 with the dashed lines. Compared to the reference model without iteration we find only minor deviations for those variables which specify the disk structure (most important are the midplane temperature $T_{\rm c}$ and

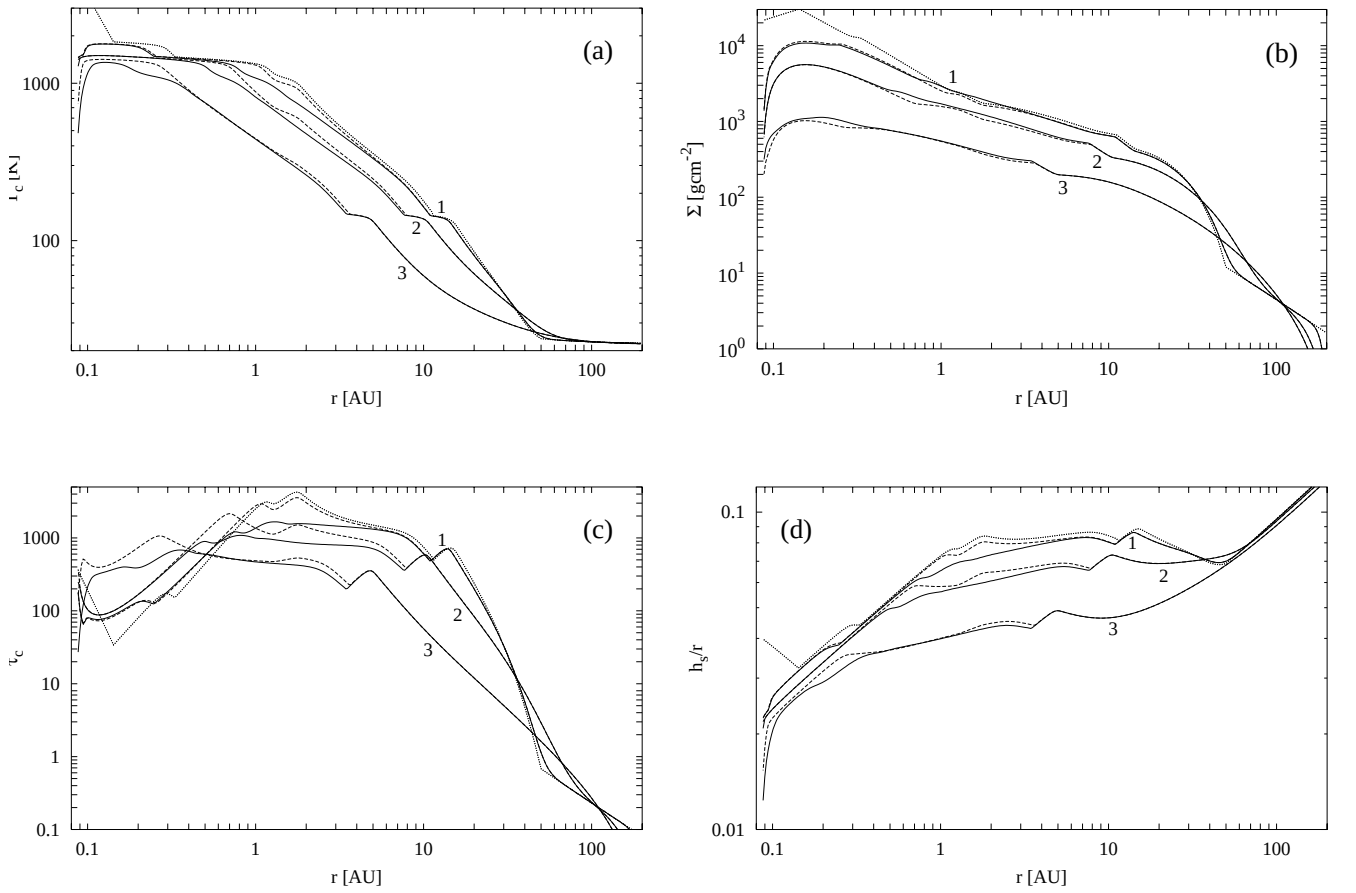

Fig. 3. The radial disk structure of model a3 with annealing, carbon combustion and radial mixing by diffusion (full lines) and without (dashed lines) after 10^4 yrs (1), 10^5 yrs (2) and 10^6 yrs (3). The initial model is indicated by dotted lines. **a)** Midplane temperature T_c. **b)** Surface density Σ. **c)** Vertical optical depth τ_c at midplane. **d)** Aspect ratio h_s/r.

surface density Σ), at a level of at most one per mille. Other variables, like the degree of condensation of the different dust species f_j and the accompanying dust opacities κ_j, differ only slightly from their values within the reference model. The differences are well below of 1% in most regions of the disk, except for the range of vapourisation of the dust species where somewhat larger deviations of more than 10% occur for these variables as compared to the reference model. Such large deviations, however, occur only if the absolute numerical values of the f_j are very low. The iterated concentrations $c_{i,\mathrm{car},k}$ and $c_{i,\mathrm{for},k}$ show a similar behaviour.

To give an example, the deviation of the degree of crystallisation $f_{\mathrm{cry,for}}$, calculated from Eq. (37), from the reference model is smaller than about 2% for $f_{\mathrm{cry,for}} \approx 10^{-3}$. At the same order of magnitude the OH particle density deviates from that of the reference model, but only in the range of OH formation. Finally, the values of the drift velocity v_r and the mass accretion rate $\dot{M}$ deviate from the reference model by roughly 15% in the vicinity of the radial grid-points, where they change sign and their absolute values become very small, while at other radial grid-points the deviation, again, is below 0.1%. We conclude from these results that the application of our semi-implicit numerical technique is of sufficient accuracy. A fully implicit calculation increases the computational time by a factor of 40 without a significant improve of accuracy.

In each model calculation we start with a time step $\Delta t = 10^{-8}$ yr and increase it slowly. The time step is chosen as follows: if the surface density changes by more than 3% between two time steps the following time step is somewhat reduced. If the change of the surface density is less than 1% the time step is somewhat increased. After an initial transient time the concentrations $c_{i,j,k}$ do not change too much if the model has relaxed from the start model and evolves steadily towards its asymptotic solution. Hence, we can take advantage of the semi-implicit method which in principle allows an unlimited increase of the time step. However, experience taught us to limit the time step to a few hundred years because of the nonlinear coupling between the model equations.

The model integration is terminated at 10^6 yr for each of the models, since our model assumptions of neglecting coagulation and formation of big bodies certainly becomes invalid after this time.

The radial grid ranges between 8.58×10^{-2} and 200 AU. The grid is chosen to be logarithmic equidistant, getting closer spaced inwards, with a resolution of 100 grid points per decade. We tested model a3 with higher and lower resolutions of 200 and 50 grid points per decade,

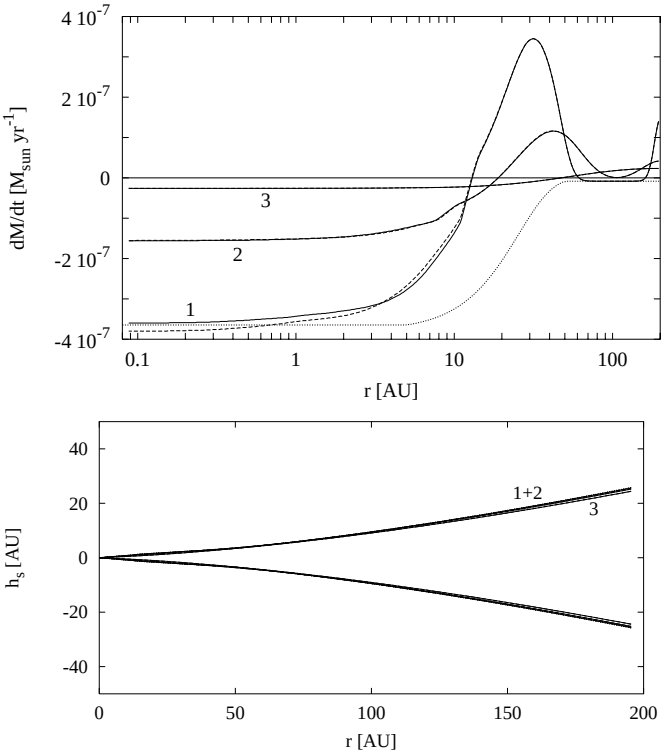

Fig. 4. The mass accretion rate $\dot{M}$ (top) and the pressure scale height h_s versus radial distance plotted with a linear scale (bottom) of model a3 with annealing, carbon combustion and radial mixing by diffusion (full lines) and without (dashed lines) after 10^4 yrs (1), 10^5 yrs (2) and 10^6 yrs (3). The dotted lines indicate the initial model.

respectively. As well we tested model a3 with larger grids for the degree of crystallisation (21 instead of 11 grid points) and for the carbon grain size (61 instead of 31 grid points). In all cases we found only minor changes as compared to the reference model which are of the order of at most a few percent for each variable.

5. Results

5.1. Time dependent radial disk structure

First we discuss the global structure of the disk for our standard model a3. Figure 3 shows the results for some important disk quantities. They are compared with the results of a model calculation with the same set of parameters for the disk, but neglecting annealing of silicate, carbon combustion and radial mixing of silicate and carbon grains in the disk.

At first we notice in Fig. 3 the steady depletion of the disk due to the accretion process which lowers the midplane temperature T_c (Fig. 3a) and the surface density Σ (Fig. 3b) with time. After 10^6 yr the disk mass is reduced from initially 0.2 to 0.095 $M_\odot$. Associated with the disk depletion is the slow inward shift of the vaporization lines of the most important absorbers which clearly can be seen in the time dependent evolution of the midplane optical depth τ_c (Fig. 3c) and especially in the inward shift of the temperature plateaus, which results from the opacity reduction by dust vaporization. These effects already are observed in the time dependent model calculations of Ruden & Pollack (1991).

The comparison of the results of model a3 with and without radial mixing by diffusion confirms the results of Paper I. The global disk structure decisively is modified by the annealing of silicate grains, but only in the inner part of the disk, where silicate dust is one of the main absorbers.

As a result of silicate annealing the midplane temperature is lowered and the surface density increases significantly in the region where silicate dust exists. As an example of the maximum deviation between both models, i.e. between the models neglecting or including annealing, the surface density after 10^5 yr at 0.65 AU is increased by $390\,\mathrm{g\,cm^{-2}}$ from 1820 to $2210\,\mathrm{g\,cm^{-2}}$ and the midplane temperature is reduced by 230 K from 1310 to 1080 K. The consequences for chemical processes within the disk due to the temperature reduction will be the subject of future investigations.

In the outer zones the disk atmosphere is not optically thick anymore. The point of transition from the optically thick to the optically thin case first moves from 48 to 70 AU by the radial expansion of the disk during early evolutionary stages, later the transition point moves inwards again because of disk clearing. In principle, for optical depths below unity the present model is inconsistent because our calculation of the midplane temperature (27) assumes optical depths exceeding unity. However, the disk structure within the inner part of the disk might not be effected too much by this.

Figure 3d shows the influence of annealing on the aspect ratio h_s/r. In model a3 there might exist two zones of shadowing of the disk surface against illumination by the protosolar radiation field that are located outwards and close inwards of the vaporization line of ice[6]. Furthermore, in the model neglecting silicate annealing, carbon combustion and radial mixing there might occur additional zones of shadowing, after 10^4 yr at 1.2 and 2.5 AU and after 10^5 yr at 1.0 AU. However, the model including silicate annealing, carbon combustion and radial mixing does not show these additional zones of shadowing, since in this case the radial run of the aspect ratio h_s/r is more smooth. Presently we do not consider stellar irradiation of the disk surface in our model calculation, though this is important for the chemical composition of the disk, because the vertical mixing in turbulent regions of the disk transports chemical processed matter from the surface to the midplane and vice versa. However, such effects can not be treated on the basis of the one zone approximation.

The upper part of Fig. 4 shows the time evolution of the mass accretion rate. In the inner part of the disk

[6] Note that the aspect ratio is not a strong indicator for shadowing.

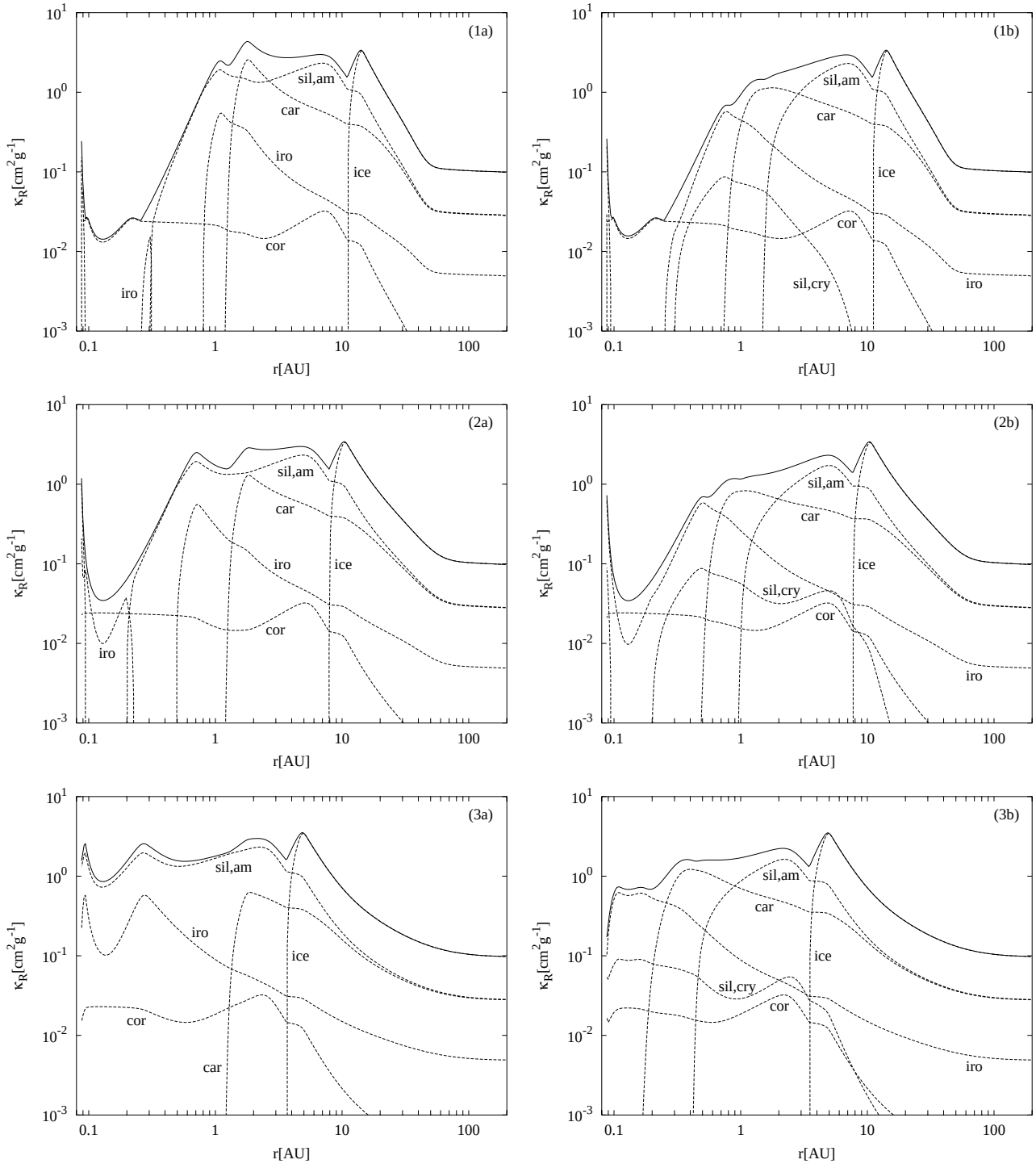

Fig. 5. Rosseland mean of the extinction coefficient $\kappa_{\rm R}$ (thick lines) after 10^4 yrs (1), 10^5 yrs (2) and 10^6 yrs (3) in model a3. The individual absorbers (dashed lines) are denoted by obvious abbreviations. *Left column:* **a)** radial mixing, annealing and carbon combustion excluded. *Right column:* **b)** radial mixing, annealing and carbon combustion included.

matter is transported inwards by viscous accretion[7]. At the same time the outer part of the disk expands due to the transport of matter outwards. The turn over point between accretion and expansion moves from 13 AU at 10^4 yr up to 47 AU at 10^6 yr. The absolute value of the accretion rate gradually decreases during the evolution of the disk. Apart from the very beginning the mass accretion rate never exceeds $3 \times 10^{-7}\,M_\odot\,{\rm yr}^{-1}$ during the evolution of the disk in model a3. Though considering or neglecting radial mixing processes in the disk considerably changes

[7] Within some turbulent eddies there probably occurs radial outflow in the midplane and accretion only in higher layers, but the off-center accretion over compensates the negative accretion in the midplane in these eddies (see the 2D models of Kley et al. 1993).

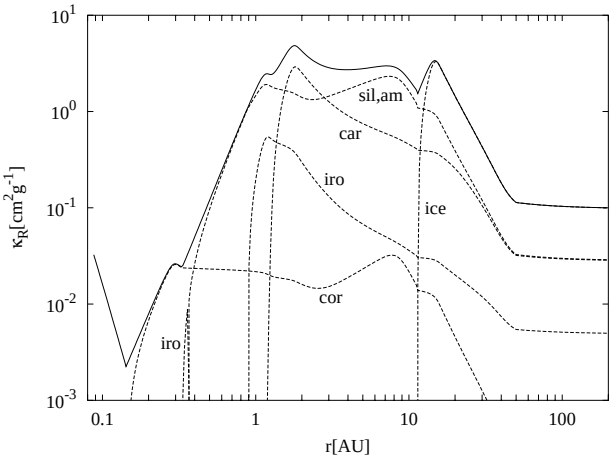

Fig. 6. Rosseland mean of the extinction coefficient $\kappa_{\rm R}$ (full line) for the initial state of the disk of model a3. The individual absorbers (dashed lines) are denoted by obvious abbreviations.

the structure of the disk model, the influence of radial mixing processes on the evolution of the mass accretion rate is small, especially in the late phases of the disk evolution.

Quite interesting is the linear-linear plot of the pressure scale height $h_{\rm s}$ versus the central distance r in the lower part of Fig. 4. The axes use the same scaling, therefore the plot represents the vertical cross section of the disk. It is remarkable that the disk's height hardly changes with time. This is a result we found for each of our models which reflects the fact that (i) according to Eq. (20) for given r the height essentially is determined by $T_{\rm c}$ and (ii) that $T_{\rm c}$ becomes nearly constant ($=T_{\rm cloud}$) in the outermost part of the disk (cf. Fig. 3a). Note that the pressure scale height is not an observable, although actually an observer's experience is that one cannot conclude the age of a protoplanetary disk from the disk geometry.

Figure 5 shows the temporal evolution of the radial dependence of the total Rosseland mean of the extinction coefficient $\kappa_{\rm R}$ for model a3 with and without radial mixing. The initial profile of $\kappa_{\rm R}$ is shown in Fig. 6. The individual contributions of the most important absorbers are plotted in both figures, too. The comparison of the left and the right part of Fig. 5 reveals the strong modification of the disk opacity by silicate annealing. By annealing, the total extinction coefficient drops by more than a factor of 2 in the zone of dominant silicate absorption. The extinction of the other absorbers also is changed by the modified temperature and density conditions within the disk. The influence of radial mixing on the radial distribution of annealed silicate dust grains is evident. Crystalline grains are present even in low temperature regions of the disk, though annealing only occurs at temperature above $\approx$800 K. More details are discussed below.

Comparing our present results with the stationary models of Paper I reveals the importance of time dependent calculations, particularly for the extinction properties of the disk (cf. Figs. 6 and 5 of the present work with Fig. 3 in Paper I). The result for the stationary disk models of Paper I are not merely snapshots of the disk in some evolutionary stage but correspond to virtual final stages of stationary disks where diffusion has operated for infinitely long times. Real disks, however, exist only for a limited period of time of at most 10^7 yr (Strom et al. 1993; Hartmann et al. 1998; Calvet et al. 2000) shorter than the characteristic diffusion time scales in the outer part of the disk (cf. Fig. 9 of Paper I). This results in a significantly different extinction structure of the evolved disks for the time dependent models of our present work compared to the stationary models of Paper I.

In addition, it is noteworthy that in our standard model a3 including silicate annealing, carbon combustion and radial mixing for each of the main dust absorbers there exists a radial zone in the disk, where this absorber dominates the disk's opacity. E.g., at 10^4 yr the main absorber for $r \geq 12$ AU is ice coated dust, for $2.8\,{\rm AU} \leq r < 12\,{\rm AU}$ amorphous silicate dust, for $1.0\,{\rm AU} \leq r < 2.8\,{\rm AU}$ carbon dust, for $0.3\,{\rm AU} \leq r < 1.0\,{\rm AU}$ iron dust and for $0.1\,{\rm AU} \leq r < 0.3\,{\rm AU}$ corundum dust, respectively. This is a consequence not only of the different stability limits of the different dust species, but also of the particular initial conditions in model a3, which lead to a zone of dominant carbon absorption. Only the crystalline silicate dust shows no such zone of opacity dominance in model a3, since already the opacity of iron grains exceeds that of the crystalline silicates at 10^4 yr at each r.

Note that in the model without annealing and diffusion and also in the initial model there appears a distinct iron feature inside the radius where one would naïvely suppose complete vaporization of iron grains (see Figs. 6 and 5). This feature appears because in the region of silicate vaporization the disk temperature rises only slightly whereas the density rises strongly. This leads to a small range of stability for solid iron in our model without annealing and diffusion, whereas the model including annealing shows no such iron feature owing to the modified temperature and density conditions.

5.2. Dust behaviour in the disk

Next we consider the behaviour of the dust species in the disk for our standard model a3. For this purpose in Fig. 7 the temporal variation of the degrees of condensation of the different dust species are plotted.

The time dependent model results in a continuous transport of matter inwards due to advection and turbulent diffusion. Consequently the combustion line of solid carbon (Fig. 7a) and the vaporization lines of the mineral dust species (Figs. 7b, c and d) shift inwards with time. Corundum (Fig. 7d), for example, is stable all over the disk after 10^6 yr since, then, the maximum temperature in the disk everywhere drops below the vaporization limit of corundum (about 1800 K under the conditions of protoplanetary disks). Simultaneously with the inward drift of matter in the inner disk regions one observes the expansion of the outer parts of the disk. During the disk

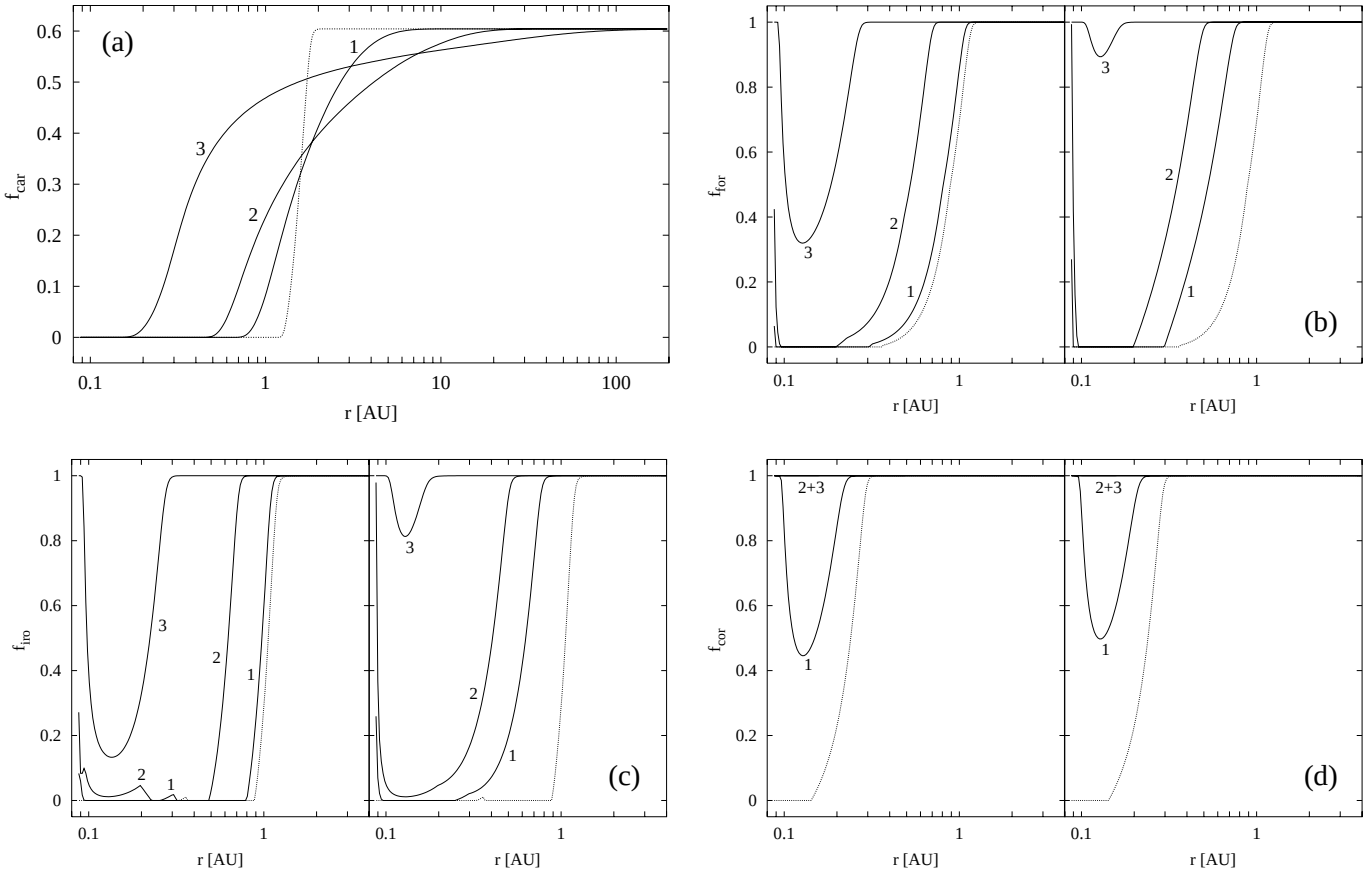

Fig. 7. Degree of condensation of the dust species after 10^4 yrs (1), 10^5 yrs (2) and 10^6 yrs (3) in model a3. **a)** Fraction of C condensed into solid carbon $f_{\rm car}$. **b)** Fraction of Si condensed into forsterite $f_{\rm for}$. **c)** Fraction of Fe condensed into solid iron $f_{\rm iro}$. **d)** Fraction of Al condensed into corundum $f_{\rm cor}$. In **b)**, **c)** and **d)** annealing, carbon combustion and radial mixing is neglected in the left and included in the right part of the figure. The dotted lines indicate the initial model.

evolution the carbon grains in the outer regions are diluted by mixing with carbon free material from the interior due to diffusive mixing. In addition, outwards of the turn over point between accretion and expansion, the outwards directed advection is the dominant transport process, which becomes important for the radial mixing of carbon grains at late times of the disk evolution.

Results of model a3 for the case where radial mixing, annealing of silicates and carbon combustion are neglected are shown in the left part of Figs. 7b, c and d. A comparison of the left and right part of the figures shows the effect of annealing of forsterite. The reduction of the opacity $\kappa_{\rm R}$ and the resulting reduction of the midplane temperature $T_{\rm c}$ by annealing leads to an inward shift of the condensation lines of the dust species. Anewed the small islands of iron stability in the innermost disk region, already mentioned above, can be seen.

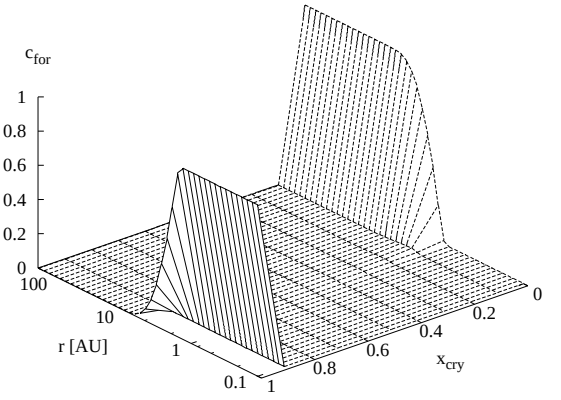

Fig. 8. Radial variation of concentration of forsterite grains $c_{\rm for}$ with different degrees of crystallisation $x_{\rm cry}$ at distance r after 10^4 yr for model a3.

Figures 8 and 9 show the distribution of annealed silicate dust in the disk for model 3 (for comparison see Figs. 5 and 6 in Paper I). Figure 8 shows the concentration of silicate grains with different degrees of crystallisation at each radius of the disk after 10^4 yr. Owing to an identical treatment of annealing in this work and in Paper I the results in the present work for annealing remain unmodified: in hotter parts of the disk where $T_{\rm c} \gtrsim 800\,{\rm K}$ the silicate is completely annealed. The turbulent mixing within the disk leads to a transport of annealed silicate dust up to large distances from the protostar which in our solar system correspond to the Kuiper belt. There exists only a small fraction of only partially crystallised silicates. The total fraction of partially crystallised forsterite takes its maximum of 4.2% after 10^4 yr at 1.8 AU. Afterwards, this maximum slowly drifts inwards (2.5% at 1.2 AU after

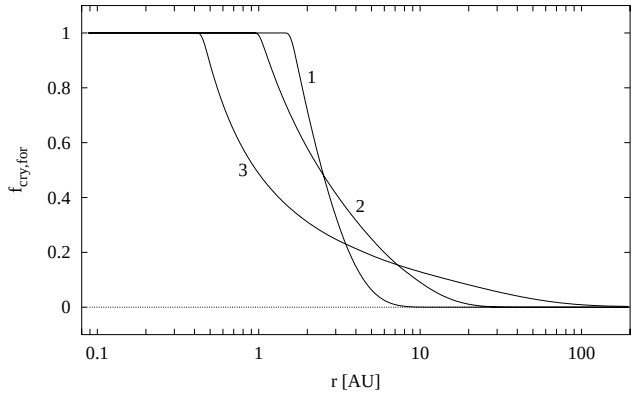

Fig. 9. Radial variation of the degree of crystallisation $f_{\rm cry,for}$ after 10^4 yrs (1), 10^5 yrs (2) and 10^6 yrs (3) in model a3. $f_{\rm cry,for}$ is dominated by grains with completely amorphous or completely crystallised lattice structure. The dotted line corresponds to the initial model.

10^5 yr and 3.4% at 0.5 AU after 10^6 yr). The maximum fraction of partly crystallised silicate occurs if the fraction of fully crystallised grains is between 80 and 90 %. In the inner parts of the disk virtually every forsterite grain is annealed.

Figure 9 shows the average degree of crystallisation $f_{\rm cry,for}$. The time dependent behaviour of annealing can be seen much clearer in this figure. Owing to the small amount of partially crystallised forsterite grains Fig. 9 approximately corresponds to the fraction of fully annealed grains in Fig. 8. As can clearly be seen, some fraction of crystallised grains is carried over a wide distance into the outer disk region after they have experienced an annealing event in the warm inner disk. After 10^6 yr, at $r = 15$ AU, the average degree of crystallisation equals about 10% ($T_{\rm c} = 43$ K) and still about 1% at 95 AU ($T_{\rm c} = 23$ K). Note that the degree of crystallisation has only a formal meaning in disk zones where silicates are completely vaporized. Of course, the numerical values given above should be taken not too seriously for our simplistic one-dimensional disk model, however, they give a qualitative clue to how substantial turbulent diffusion is able to transport matter through the disk.

We also re-calculated the model a3 with a slightly different value for the activation energy of annealing $E_{\rm a}/k_{\rm B} = 41\,000$ K which was derived by Lenzuni et al. (1995) and Duschl et al. (1996) from the annealing experiment of Nuth & Donn (1982). As a result of the higher activation energy the fraction of crystalline silicates in the disk slightly decreases which results in a slight increase of the opacity as well as of the midplane temperature. The maximum temperature deviation is about 10 K in the range of $T_{\rm c} = (800 \pm 50)$ K where annealing takes place. In other disk regions the modification of the disk structure is negligible. The model results, thus, do not depend critically on the value of $E_{\rm a}$.

In an annealing experiment (Hallenbeck et al. 1998; Hallenbeck et al. 2000) there has been observed a different evolutionary track of annealing of magnesium silicates as compared to the experiments of Fabian et al. (2000) and of Nuth & Donn (1982). Hallenbeck et al. 1998 detect a stall phase within the annealing process, during which the spectral features of the silicates at 10 μm hardly change. The stall phase might be attributed to a different composition of the initial amorphous silicates as compared to those of Fabian et al. (2000) and of Nuth & Donn (1982). As a result the characteritic timescale of annealing has a different form as compared to (7), and the annealing temperature increases from about 800 K to about 950 K in the present disk models. Though we did no time dependent model calculation with the law for the characteritic timescale of annealing of Hallenbeck et al. (2000), we conclude that the disk structure would be somewhat influenced in the sense that the annealing zone is slightly shifted inwards, but it does not dependent critically on the annealing model.

We also continued the calculation of model a3 after 10^6 yr up to a time of 5×10^6 yr. Besides the further depletion and cooling of the disk the radial mixing of matter in the disk progresses during this period of disk evolution. As a consequence of diffusional mixing and outwards directed advective transport in the outer parts of the disk, the radial run of the degree of crystallisation of forsterite $f_{\rm cry,for}$ markedly flattens at 5×10^6 yr. For example, $f_{\rm cry,for}$ drops to 0.150 at 1 AU and increases to 0.084 at 100 AU at this instant (cf. Fig. 9). At the same time the degree of condensation of carbon grains $f_{\rm car}$ is even almost a constant of roughly 0.58 throughout the entire disk (cf. Fig. 7a). The disk mass decreases to $0.016\,M_\odot$ at 5×10^6 yr.

Figure 10 shows the change of the radial variation of the carbon grain size distribution with time. The initial grain size spectrum (Fig. 10a) was constructed from the stationary disk model including combustion but neglecting annealing and diffusion. At ∼1.7 AU the initial size distribution of carbon grains in the small zone of carbon combustion can clearly be seen. During the subsequent disk evolution the initial grain size spectrum changes gradually due to carbon combustion and radial mixing of the disk matter (Figs. 10b, c and d). As an important effect the concentration of solid carbon in the outer disk decreases because the carbon grains are diluted by mixing with carbon free gas from the inner disk regions (cf. Fig. 7a). However, the variation of the exponent of the size spectrum $\beta_{\rm MRN}$ with time is negligible, except in the zone of complete carbon combustion where the size distribution flattens markedly until finally the largest grains disappear.

Figure 11 shows the radial run of the partial pressure of OH, which is responsible for the oxidation of the carbon grains, and the total gas pressure. OH is sufficiently abundant to oxidize carbon only in the innermost part of the disk. Combustion sets in if the particle pressure of OH exceeds about $10^{-10}\,{\rm dyn\,cm^{-2}}$, which corresponds to a midplane temperature of about 1100 K in the present models. The characteristic time of combustion (4) of a carbon grain with a radius of 0.25 μm then is of about 3×10^4 yr.

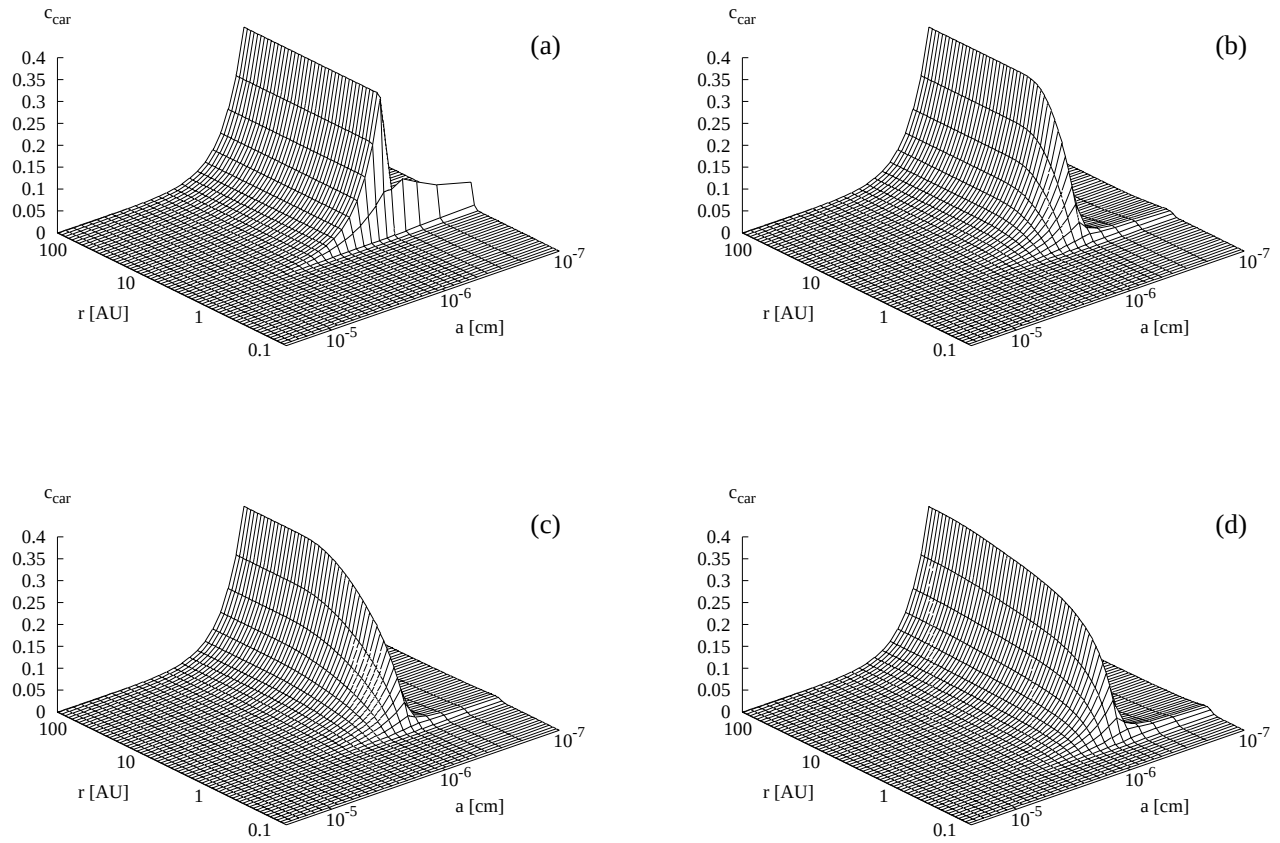

Fig. 10. Radial and time dependent variation of the carbon grain size spectrum. $c_{\rm car}$ is the concentration of carbon grains of radius a at distance r for model a3 for the initial model (initial MRN distribution) **a)** and after 10^4 yrs **b)**, 10^5 yrs **c)** and 10^6 yrs **d)**, respectively.

Finally, Fig. 12 shows the temporal variation of two selected disk variables, the midplane temperature $T_{\rm c}$ and the degree of crystallisation of forsterite $f_{\rm cry,for}$, at selected radial distances from the protostar $r = 1$, 3, 5, 10 and 30 AU for model a3. These radii roughly correspond to the present positions of the Earth, the asteroid belt, Jupiter, Saturn and Neptune, respectively.

The midplane temperature $T_{\rm c}$ in model a3 including silicate annealing, carbon combustion and radial mixing (Fig. 12a), again, reveals the depletion of the disk with time owing to accretion onto the star. However, as the accretion rate decreases with time (Fig. 4a), the decrease of the midplane temperature slows down. For example, this leeds to midplane temperatures of 30, 175 and 444 K after 10^6 yr at the locations of Neptune, Ceres and the Earth, respectively. The plateaus at the graphs for 5 and 10 AU are due to the vaporization of ice. These plateaus are instructive and may be important for the formation of the gas planets since in model a3 at the distance of Jupiter, for example, the midplane temperature remains roughly constant at about 140 K from 3.5×10^5yr on for many of hundred thousand years.

The time evolution of the degree of crystallisation of forsterite $f_{\rm cry,for}$ in model a3 at different radial distances (Fig. 12b) shows a division into three radial zones of different type of time evolution within the first 10^6 yr. In the inner part of the disk ($r \lesssim 2$ AU) from the very beginning on all the silicate grains are annealed, and they remain to be so as long as the temperature is higher than 800 K, whereafter $f_{\rm cry,for}$ decreases with time due to the disk depletion. In the outer part of the disk ($r \gtrsim 10$ AU) $f_{\rm cry,for}$ increases with time due to radial turbulent mixing. In an intermediate zone (2 AU $\lesssim r \lesssim$ 10 AU) first radial mixing leeds to an increase of $f_{\rm cry,for}$, whereas later the disk depletion moves the disk matter closer to the star and then reduces $f_{\rm cry,for}$. Thus $f_{\rm cry,for}$ takes a maximum and decreases afterwards. At 10^6 yr the degree of crystallisation of forsterite at the location of Ceres is of about 25%, whereas it has just reached 5.6% at the location of Neptune.

5.3. The distribution of largest experienced temperature

For studying the mineralogy of primitive meteorites and comets the temperature history of their building blocks is of great interest. For this purpose we calculate for each distance r the distribution of the highest temperatures the dust particles found at this distance ever experienced during their past history.

We approach this problem by defining a grid for the highest temperatures T_l that dust grains ever experienced in the disk, where l denotes the grid point of the temperature grid. We choose a temperature grid between

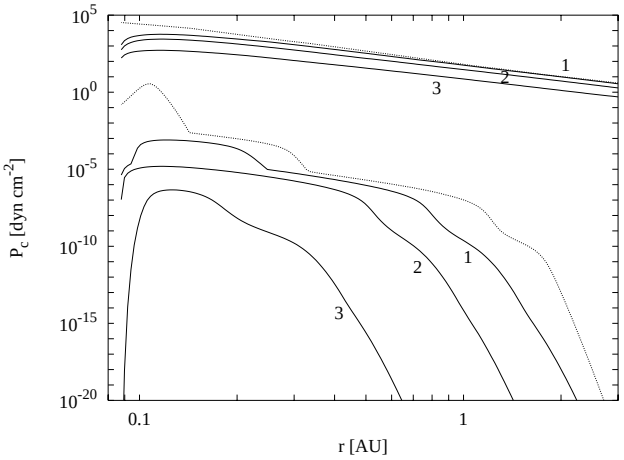

Fig. 11. Total pressure of the gas (top) and pressure of OH (bottom) at the midplane of the disk in model a3 after 10^4 yrs (1), 10^5 yrs (2) and 10^6 yrs (3). The dotted lines indicate the initial model.

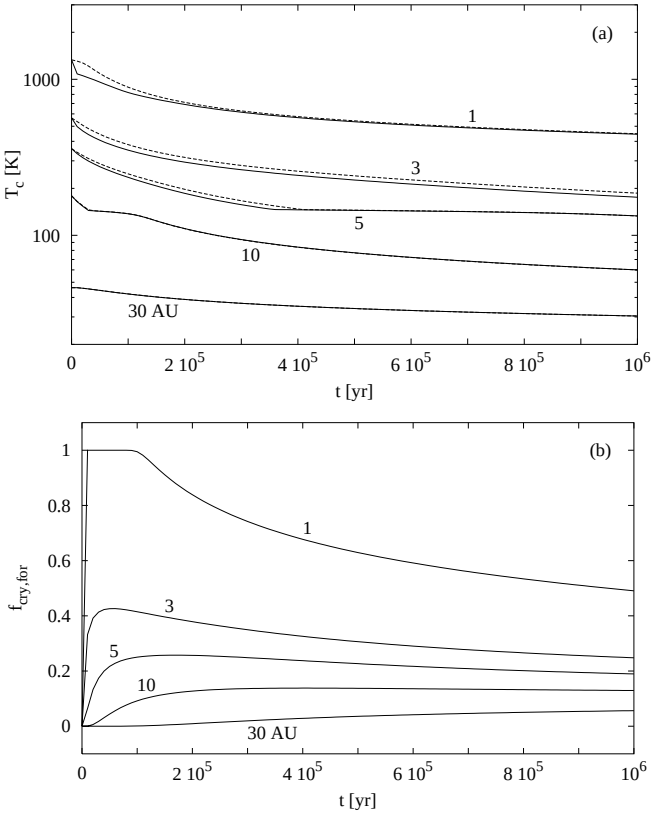

Fig. 12. The time evolution of **a)** the midplane temperature T_c and **b)** the degree of crystallisation of forsterite $f_{\mathrm{cry,for}}$ in model a3, including (full lines) and neglecting (dashed lines) silicate annealing, carbon combustion and radial mixing at selected radial distances to the protostar. These radii roughly correspond to the orbits of the Earth, the asteroid belt, Jupiter, Saturn and Neptune, respectively.

a minimum and a maximum temperature of 20 K and 2020 K, respectively, in steps of 40 K (51 grid-points). The minimum temperature equals the temperature of the ambient molecular cloud, i.e. the minimum (midplane) temperature in the disk in our models, and the choice of the maximum temperature accounts for the fact that above 2000 K the dust in the disk is completely vaporized under the conditions of the protosolar nebula.

The occupation number of each temperature grid point l at distance r denotes the fraction of dust grains $C_l(r)$, which previously have experienced a highest temperature event falling into $T_l - 20\,\mathrm{K} \le T < T_l + 20\,\mathrm{K}$. If the local dust temperature $T(r)$ satisfies

$$T(r) \ge T_l + 20\,\mathrm{K} \tag{44}$$

for some l with $1 \le l \le L$, where L is the maximum of l for which (44) is satisfied, the concentration C_{L+1} of level $L+1$ at the radius r is increased by the value of C_l and C_l is set to zero for all $l = 1 \ldots L$ satisfying (44). For the purposes of numerical calculations this behaviour is simulated by letting

$$\frac{\mathrm{d}C_l}{\mathrm{d}t} = \begin{cases} \dfrac{C_{l-1}}{\mathfrak{T}_{l,l+1}} - \dfrac{C_l}{\mathfrak{T}_{l,l+1}} & \text{if} \quad T_\mathrm{c} \ge \frac{1}{2}(T_l + T_{l+1}) \\ 0 & \text{else} \end{cases}, \tag{45}$$

where $\mathfrak{T}_{l,l+1}$ is the characteristic time of transition from level l to $l+1$.

In protoplanetary disks gains and losses at the temperature grid point l also occur by radial turbulent and advective transport. Hence, to determine the occupation numbers C_l we have to solve another set of diffusion-transport-reaction equations (cf. Eqs. (8) and (11))

$$\frac{\partial C_l}{\partial t} + v_r \frac{\partial C_l}{\partial r} - \frac{1}{rn}\frac{\partial}{\partial r} rnD \frac{\partial C_l}{\partial r} = R_l, \tag{46}$$

where the rate term R_l is given by the rhs of Eq. (45). The indices k of the radial grid are omitted in Eqs. (45) and (46) for clarity. Once again one has to observe the modification of the gain and loss terms in Eq. (46) at the borders of the l-grid (cf. Sect. 2.4).

Since gain and loss at a temperature level l occurs instantaneously we set the characteristic time of change $\mathfrak{T}_{l,l+1}$ to a small fraction of the current numerical time step Δt,

$$\mathfrak{T}_{l,l+1} = 10^{-3}\Delta t. \tag{47}$$

The set of Eq. (46) is solved by the same method as presented for the solution of the set of diffusion-transport-reaction Eq. (8) (fully implicit).

The choice of the temperature differences ΔT_l of the l-grid is constrained by the largest differences in temperature between two radial sampling points k and $k+1$. If the grid point distance within the l-grid is smaller than the temperature difference between two points of the radial k-grid, then the concentration C_l at some l can get unnaturally depleted compared to the concentrations C_{l-1} and C_{l+1}. In order to meet this requirement we re-calculated the model a3 with 200 radial grid points per decade (instead of 100 in the standard case) and found the lowest admitted value of the temperature differences ΔT_l within the temperature grid for an adequate resolution to be 40 K.

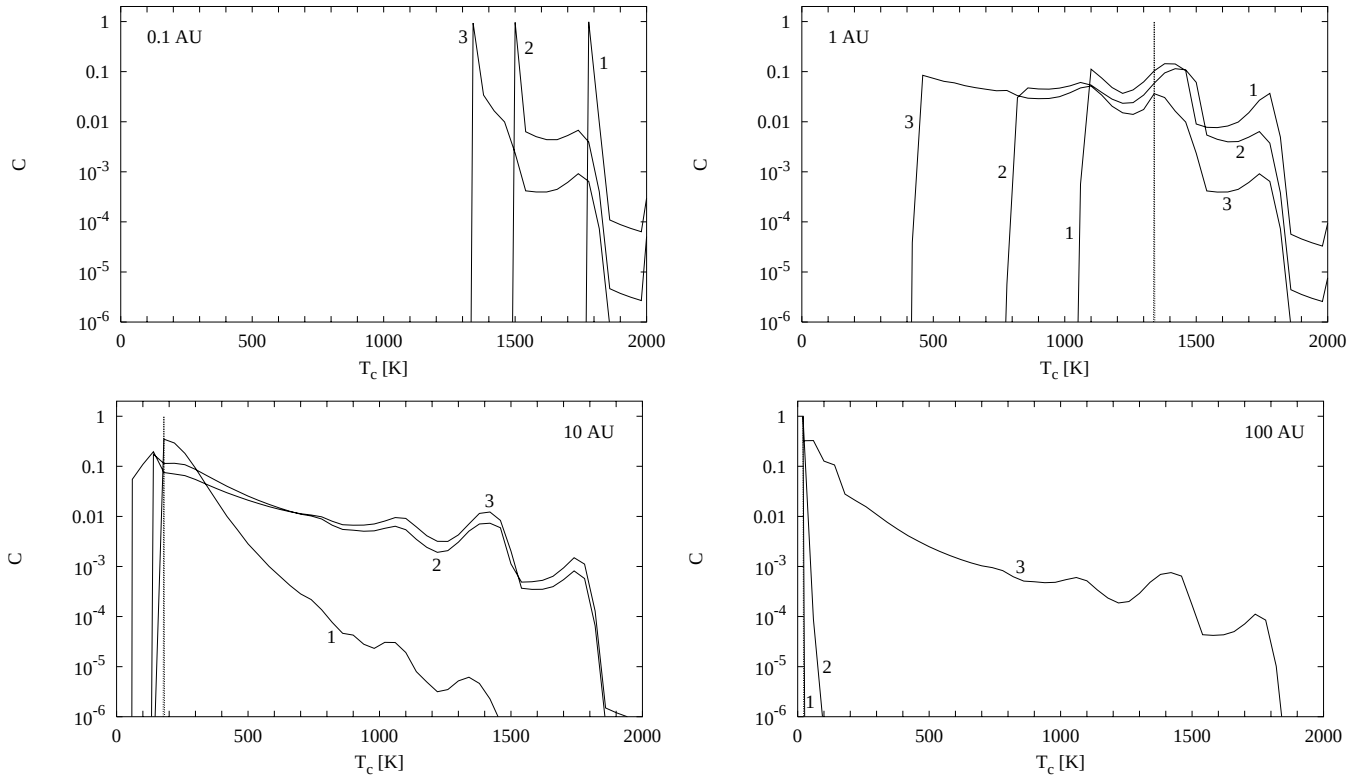

Fig. 13. The concentration of dust particles C which experienced a largest temperature T_c at the midplane of the disk in model a3 (including radial mixing) at some selected radial distances after 10^4 yrs (1), 10^5 yrs (2) and 10^6 yrs (3). The temperature of the initial model is indicated with dotted lines. *Top left:* at $r = 0.1$ AU. *Top right:* at $r = 1$ AU. *Bottom left:* at $r = 10$ AU. *Bottom right:* at $r = 100$ AU.

The result for model a3 is shown in Fig. 13. For selected radial distances the concentration distribution C_l is plotted. Loosely speaking, this shows for some temperature T_c the fraction of grains which somewhere in their past have already been in a disk zone with this temperature, but never in a hotter zone. The most conspicuous features of the distribution C_l are the local maxima at 1750, 1400 and 1060 K, respectively, observable in most of the plots in Fig. 13. They result from the temperature plateaus occurring close to the vaporization lines of corundum, silicates and the combustion line of carbon, respectively (cf. Fig. 3). In addition there appears a small bump at 750 K which results from the temperature plateau due to the annealing of silicates. Hence grains which resided for a long time in the region of one of these temperature plateaus are more frequent compared to grains which experienced another temperature history.

A large fraction of the grains during the disk evolution is mixed from the inner region to large distances from the protostar. E.g., the concentration of grains which experienced a highest temperature event between 1360 K and 1400 K after 10^6 yr is 3.4% at 0.1 AU, 3.0% at 1 AU, 1.5% at 10 AU and 0.07% at 100 AU, respectively. In addition, the fraction of particles which experienced a largest temperature event of larger than 1000 K after 10^6 yr is 100% at 0.1 AU, 34% at 1 AU, 9.2% at 10 AU and still 0.61% at 100 AU, respectively. These results for the temperature history of dust grains anew demonstrate the extent of transport of matter by radial turbulent mixing in the disk.

The fraction of "well-toasted" grains in the outer parts of the disk ($r \gtrsim 10$ AU) continuously increases during the disk evolution due to radial mixing (Fig. 13). At the same time, the fraction of grains with low highest temperature events increases in the inner parts of the disk ($r \lesssim 1$ AU) owing to the decrease of the disk's midplane temperature with time by disk depletion.

Note that for $T_c \gtrsim 1700$ K all dust species are vaporized except for corundum. Hence the local maximum at ∼1750 K solely results from corundum grains. The local maximum at ∼1400 K mainly results from crystalline silicate grains, with a small admixture of corundum grains. Carbon grains appear for $T_c \lesssim 1100$ K and finally amorphous silicate grains for $T_c \lesssim 800$ K.

5.4. The models a1 and a10

After having discussed our standard model a3 in detail we consider the models a1 and a10 with lower (10^{-3}) and higher (10^{-2}) viscosity parameter α, respectively, in order to show the dependence of our time dependent calculations on the viscosity parameter.

First we compare the disk structure of the models a1 and a10 (Figs. 14 and 15) with the model a3 (Fig. 3). The most important difference between the models is the evolutionary timescale of the disk. The larger the viscosity parameter α, the larger the accretion rate $\dot{M}$ and, thus,

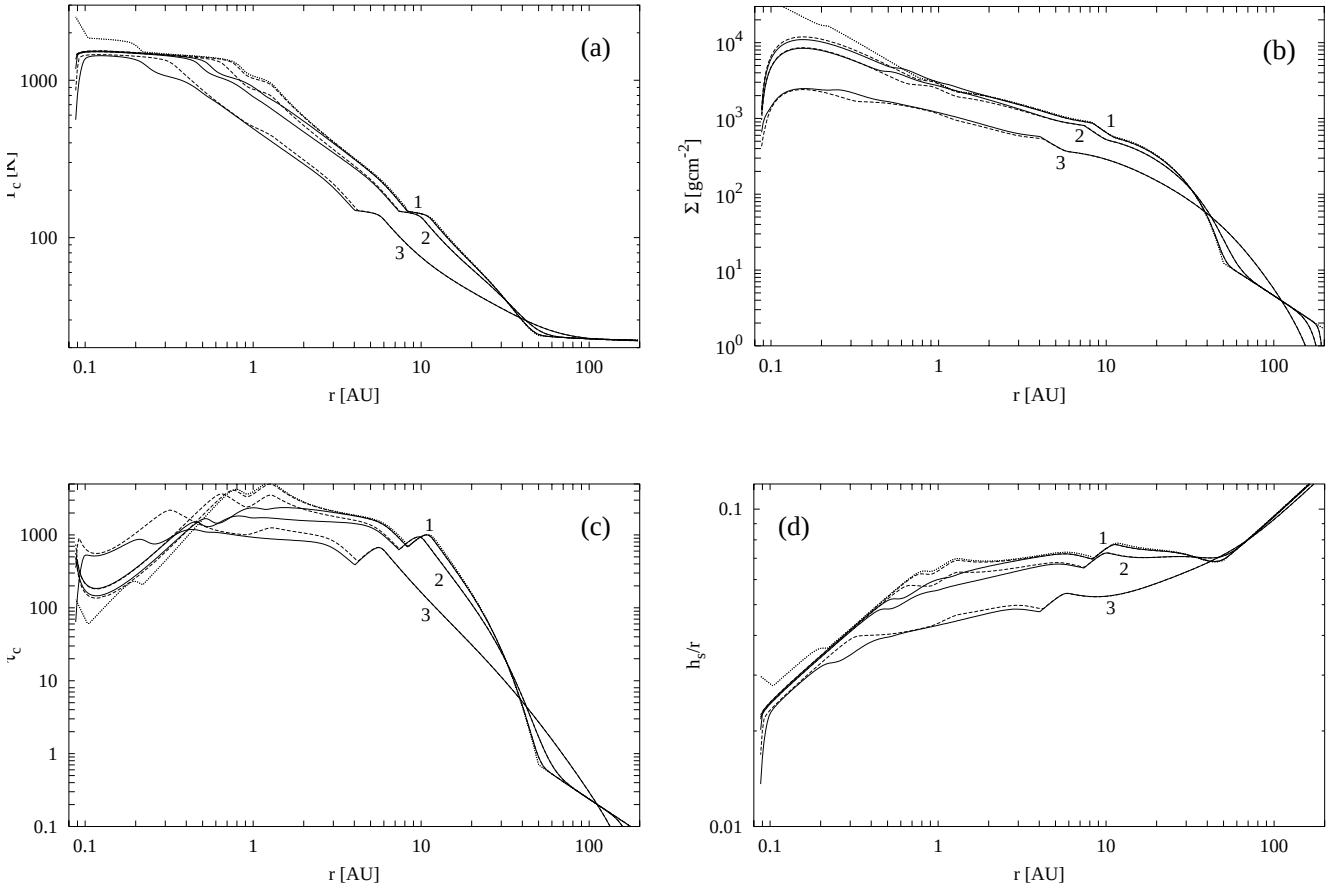

Fig. 14. Same as Fig. 3 but for the model a1 ($\alpha = 10^{-3}$).

the lower the viscous timescale. As a result the disk masses after 10^6 yr are $0.14\,M_\odot$ in model a1, $0.095\,M_\odot$ in model a3 and $0.030\,M_\odot$ in model a10, respectively.

The different extents to which the disk are depleted in the present models leads to a different time dependent evolution of their temperature and density structure. Particularly in the case of $\alpha = 10^{-2}$ the surface density distinctly drops during the late phase of disk evolution, and therefore also the midplane temperature decreases (Figs. 15a and b). In contrast, during the early phase of evolution of the disk model a10, the disk is hotter compared to the models with lower α (Figs. 3 and 14) owing to the more efficient heating by the accretion flow. Note again that the present models initially have the same disk masses and angular momenta.

Another significant property of the disk structure is the homologous time evolution of the radial dependence of the disk quantities. Particularly this property can be recognized by the inward shift of the temperature plateau corresponding to the vaporization of ice coated grains at $T_\mathrm{c} \sim 160\,\mathrm{K}$ with time (Figs. 3a, 14a and 15a). The homologous evolution of features with time results from the strong dependence of the disk structure on the opacity (Eq. (33)) which rules the radiation transport in the disk. Radiation transport in turn dominates the energy transport in protoplanetary disks (e.g. Lin & Papaloizou 1985), hence the disk structure is considerably influenced by the opacity law.

If the vertical optical depth (Figs. 14c and 15c) drops below unity, the disk gets optically thin and isothermal with respect to the z direction, i.e. the effective temperature T_eff, given by (22), equals the cloud temperature T_cloud. After $10^6\,\mathrm{yr}$, the limit $\tau_\mathrm{c} = 1$ is achieved at 69 and 31 AU for the models a1 and a10, respectively. Initially the disk is optically thin at $r > 48\,\mathrm{AU}$ for each model. Thus, at the time of termination of the simulation, model a1 has not finished its expansion phase as a result of angular momentum transport, whereas model a10 already is in the contraction phase due to substantial mass loss onto the star.

The influence of radial mixing of annealed silicates on the disk structure in both models a1 and a10 (Figs. 14 and 15) is similar to that observed in model a3 (Fig. 3). At early evolutionary stages the location of significant modifications of the disk structure as compared to the model neglecting carbon combustion, silicate annealing and radial mixing occurs, again, in the temperatures range $[200, 1450]\,\mathrm{K}$, i.e. between the vaporization lines of ice and (annealed) silicates. The magnitude of the alteration of model a1 and a10 by either including or neglecting annealing and radial mixing is of the same order of magnitude as compared to model a3, i.e. a maximal decrement of the midplane temperature T_c and increment of the surface density Σ of about 25% for model a1 and 15% for model a10. The vertical optical depth is reduced by a factor of roughly 2 in maximum. The radial run of the aspect

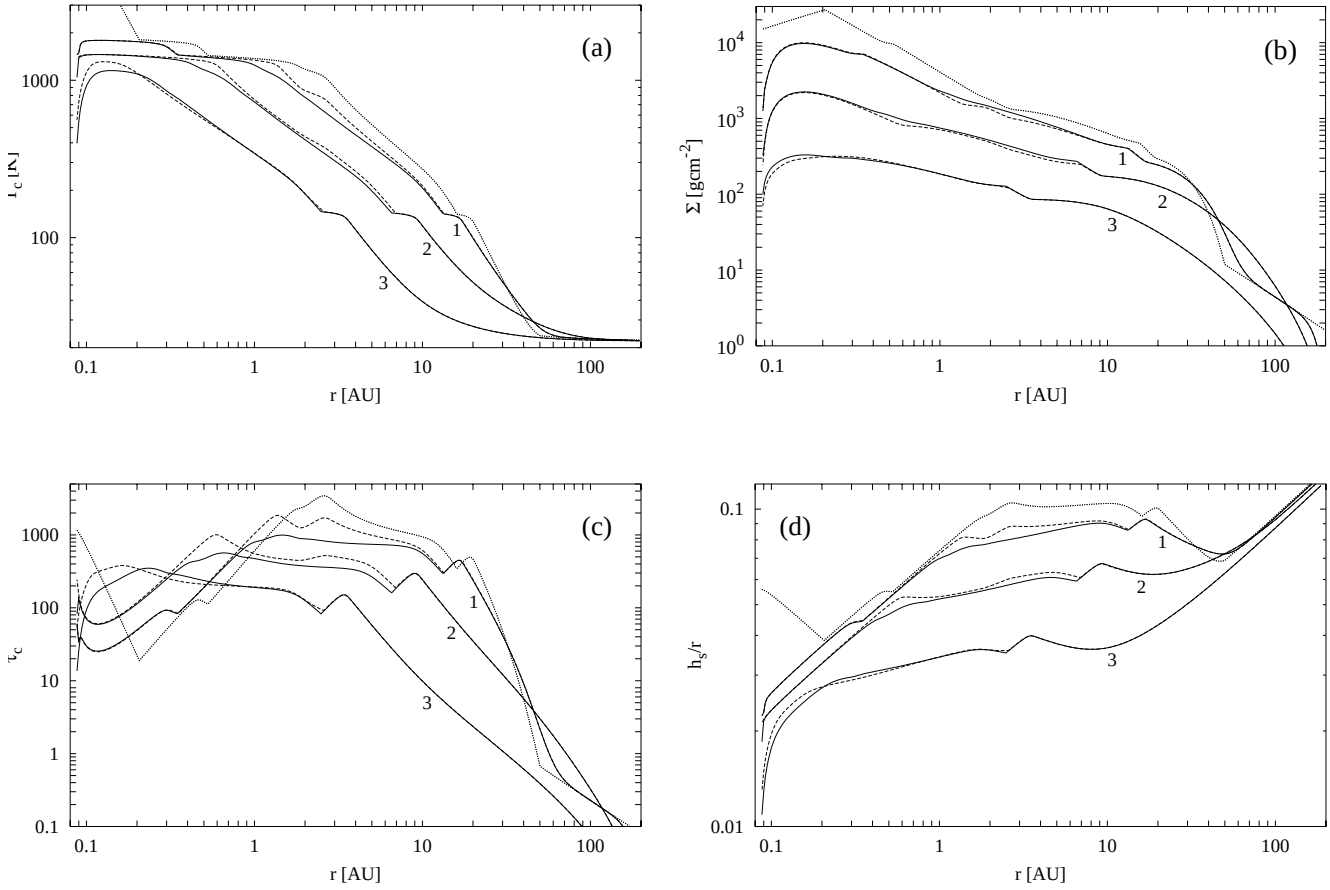

Fig. 15. Same as Fig. 3 but for the model a10 ($\alpha = 10^{-2}$).

ratio h_s/r in both models a1 and a10 shows a smoothing similar to model a3 with the exception that in model a1 including annealing, carbon combustion and radial mixing there might occur an additional shadowing zone, which is located at 0.6 AU after 10^4 yr and at 0.5 AU after 10^5 yr, respectively.

In Fig. 16 the results for the time dependent behaviour of important dust species for both models a1 (I) and a10 (II) are shown. Figures 16 Ia and IIa show the degree of condensation of carbon for both models. Obviously the different values of the viscosity parameter α leed to a more rapid evolution of the disk of model a10 compared to the the disk of model a1. Whereas in model a1 solid carbon is completely oxidized inside of 0.2 AU at 10^6 yr (Fig. 16 Ia), in model a10 the stability limit of carbon has moved below the inner boundary of the radial grid at the same time (Fig. 16 IIa). At the same time oxidation products of carbon combustion are transported up to the outer boundary of the radial grid after 10^6 yr in model a10 (Fig. 16 IIa). This is not a result of diffusive mixing, since the viscous timescale $\tau_\nu = r^2/\nu$ in the outer parts of the disk exceeds the termination time of the model calculation, but is a result of the outward advection in the outer disk zone. The turn over point between accretion and expansion at 10^6 yr in model a10 is located at 49 AU, and the viscous timescale τ_ν at 200 AU, for example, remains roughly constant at 2.7 Myr during the disk evolution. Hence, the degree of condensation of carbon slightly drops below the initial value of 0.6 after 10^6 yr in the outer parts of the disk, because of the outward transport of carbon free material by disk expansion. In contrast, owing to the lower value of α the disk model a1 after 10^6 yr has not evolved to such an extent that a substantial fraction of partially burned material is transported to the outer boundary.

Figures 16 Ib and IIb show the time dependent evolution of the degree of condensation of forsterite for both models a1 and a10. The degree of condensation of forsterite becomes unity for radii larger than 1 AU in both models after 10^4 yr (Figs. 16 Ib and IIb). At 10^6 yr forsterite is condensed even everywhere in model a10 within the range of our radial grid (Fig. 16 IIb), while disk model a1 is hot enough at this instant to vaporize a certain fraction of the silicate in the inner part of the disk. Note that initially the stability limits of solid carbon and of the silicates in model a1 are at different locations compared to model a10.

In Figs. 16 Ic and IIc the evolution of the degree of crystallisation of forsterite with time is plotted for models a1 and a10. The transport of annealed silicates across the disk by diffusional mixing is remarkable. In both models a substantial fraction of crystallised silicate grains spreads across the optically thick part of the disk at termination of the simulation. Up to 10^6 yr the degree of crystallisation at $\tau_c = 1$ is 2.5×10^{-4} in model a1 (69 AU) and

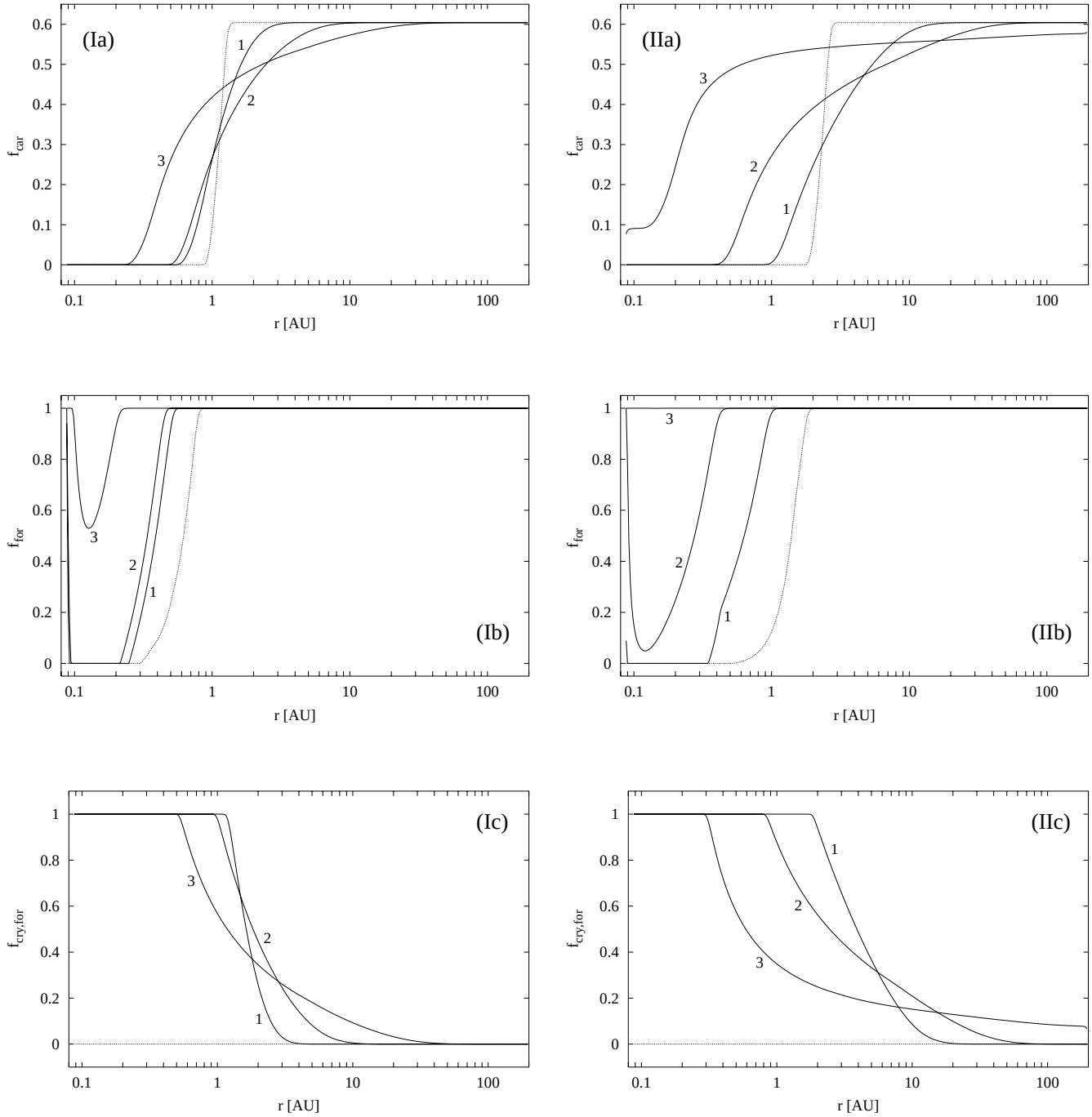

Fig. 16. Degree of condensation of carbon **a)**, degree of condensation of forsterite **b)** and degree of crystallisation of forsterite **c)** after 10^4 yrs (1), 10^5 yrs (2) and 10^6 yrs (3) in model a1 with $\alpha = 10^{-3}$ (I) and a10 with $\alpha = 10^{-2}$ (II). The initial model is indicated with dotted lines.

0.115 in model a10 (31 AU), respectively. At the same instant within the asteroid belt the degree of crystallisation exceeds 17% in each model.

6. Concluding remarks

Protoplanetary accretion disks are fascinating objects, not only for observers, but also from the theorists point of view. Their theoretical interpretation and model construction even in the simplest case require the simultaneous application of several physical theories: mechanics, hydrodynamics, turbulence theory, thermodynamics, solid state physics, optics, radiation transport theory and chemical reaction theory, respectively.

In the present work we try to insert a further building block into the still incomplete building of the theory of the properties and evolution of protoplanetary accretion disks and of the solar nebula: time dependent radial mixing of particulate disk species, which are of interest with respect to the evolution of the disk structure, to observations of protoplanetary disks and to primordial bodies in the solar system.

It is known from the observations of IR spectra of comets that some comets contain a substantial fraction of crystalline silicates. By fitting laboratory spectra of a number of candidate minerals in the spectral range of $8-13\,\mu$m, Hanner et al. (1994b) obtain good agreement with the spectra of comets P/Halley (1986 03), Bradfield (1987 29) and Levy (1990 20), respectively, by assuming a fraction of roughly 25% crystalline olivine embedded within a matrix of amorphous olivine. Similar fractions of crystalline olivine are found to be present in the comets Mueller (1993a) (Hanner et al. 1994a) and Hale-Bopp (1995 O1) (Crovisier et al. 1997; Hanner et al. 1997; Bouwman et al. 2001). Recently Yanamandra-Fisher & Hanner (1999) anewed fit the spectra of the above comets by using optical properties of nonspherical particles. Their calculation gave best fit for a mixture of amorphous and crystalline olivine grains with a fraction of 20% crystalline olivine. Also remarkable is the comet 103P/Hartley 2, which likewise exhibits the crystalline silicates bands in its IR spectrum (Crovisier et al. 1999b), but which suppose to originate from the Edgeworth-Kuiper belt in contrast to the above comets which originate from the Oort cloud.

By assuming that annealing and radial mixing is the process explaining the presence of crystalline olivine in comets, our model results favour a not too low viscosity parameter α, as a degree of crystallisation of silicates $f_{\rm cry,for} \geq 0.2$ outside of the snow line ($T_{\rm c} \lesssim 160\,{\rm K}$), where the cometesials were formed, is attained only by the models a3 ($\alpha = 3 \times 10^{-3}$) and a10 ($\alpha = 10^{-2}$) during a long period of the disk evolution. For models a3 and a10 a degree of crystallisation of 20% in the region of ice stability is achieved after roughly $3 \times 10^5\,{\rm yr}$ and $5 \times 10^4\,{\rm yr}$, respectively. As a result, comets which contain this fraction of crystalline silicates have to be formed inside of about 7 AU in model a3 and about 11 AU in model a10. In contrast, for the model a1 with $\alpha = 10^{-3}$ the degree of crystallisation just attains 20% close the vapourisation line of ice at the time of termination of the simulation ($10^6\,{\rm yr}$) at a radial distance of about 4.5 AU. Other comets show no features of crystalline silicates in their spectra, hence the location of their formation seems to be far outside in the disk where $f_{\rm cry,for}$ is very small.

Admittedly, the above numerical values of our model calculations should not be taken too seriously since we do not know the true initial conditions of the solar system, e.g. the initial disk mass and angular momentum. Furthermore, we do not resolve the vertical and azimuthal direction, and we still do not be aware of the true mechanism driving viscous accretion and turbulence. However, the results of our model calculations qualitatively demonstrate the efficiency of radial mixing of matter within the solar nebula. Improved future models have to be developed to verify these results.

Evidence of radial mixing and annealing in the solar nebula beside the comets also is detected in meteorites. Actually, it is not easy to find evidence in laboratory study as in most cases the building blocks of the meteorites, which are assumed to be primordial matter of the solar system, are thermally altered within the meteoritical parent bodies. As an example, the coarse grained component of the matrix of the Allende meteorite experienced a heating event that lasted about 10−100 days at a supposed temperature of 1000 K (Toriumi 1988). Annealing of the coarse silicate grains is a possible explanation. A more distinct indication for annealing in the primordial solar nebula shows the CO meteorite Allan Hills A77299. The matrix of Allan Hills contains a significant fraction of olivine that obviously was crystallised under low pressure conditions, i.e. not inside a larger parent body (Brearley et al. 1989). The authors rule out other formation processes, e.g. crystallisation during dust condensation or an impact event.

Another indication of radial mixing within the primordial solar nebula is the presence of methane in the comets. A formation of CH_4 in the cold outer parts of the disk seems to be impossible (Fegley & Prinn 1989). In our model calculation we showed that the degree of condensation of carbon grains $f_{\rm car}$ in the middle and outer zones of the disk decreases with time as a result of diffusional mixing, e.g. from initially 0.6 to 0.55 at 6 AU after $10^6\,{\rm yr}$ in each of the models (a1, a3 and a10). The carbon dust rich matter from the parent molecular cloud is diluted by carbon dust poor matter from inner disk regions which contains the combustion products of the carbon grains, especially C_2H_2 and CH_4, which are products of chemical reactions of the residuals of carbon combustion in the gas phase (Finocchi et al. 1997a). This could explain the large observed fraction of the methane and acetylene in the comets (Crovisier & Bockelée-Morvan 1999a).

Evidence of annealed silicates outside of the solar system shows the disk around TW Hya. TW Hya is an about 8 Myr old pre-main sequence star (Webb et al. 1999). In a recent observation the optically thick disk of TW Hya has been resolved in the near IR, while it still remains unresolved in the mid IR (Weinberger et al. 2002). The spectrum in the range of $10\,\mu$m clearly shows the $11.3\,\mu$m feature of crystalline forsterite and a flat shape in the region of about $10-11.5\,\mu$m similar to Hale-Bopp in April 1997 (Bouwman et al. 2001) which is typically for a mixture of amorphous and crystalline silicates. These results are a rather strong indicator for proceeded annealing in the protoplanetary disk of TW Hya, though the crystalline material could also be liberated by collisions between large planetesimals and cometesimals, respectively, which might be present in this developed disk and which experienced thermal alteration in their interiors.

In conclusion, one of the most important results of our model calculations is that radial mixing of annealed silicate grains affects the disk's radial structure to a significant extent. In the zone of stability of silicate dust in each of the models (a1, a3, a10), the inclusion of silicate annealing, carbon combustion and radial mixing reduces the midplane temperature by about 20% as compared to the models including these processes, while the surface density increases to the same percentage. This result clearly shows that annealing, carbon combustion and radial mixing can

not be neglected in model calculations of protoplanetary accretion disks, which have the purpose of investigating the radial structure, chemical composition and radiation of the disks.

Acknowledgements. This work is supported by the Deutsche Forschungsgemeinschaft (DFG), Sonderforschungsbereich 359 "Reaktive Strömungen, Diffusion und Transport", and by the Landesgraduiertenförderung Baden Württemberg.

References

Anders, E., & Kerridge, J. F. 1988, in Meteorites and the early solar system, ed. J. F. Kerridge, & M. S. Matthews (University of Arizona Press, Tuscon), 1155
Balbus, S. A., & Hawley, J. F. 1991, ApJ, 376, 214
Bell, K. R., & Lin, D. N. C. 1994, ApJ, 427, 987
Bouwman, J., Meeus, G., de Koter, A., et al. 2001, A&A, 375, 950
Brearley, A. J., Scott, E. R. D., Keil, K., et al. 1989, Geochimica et Cosmochimica Acta, 53, 2081
Cabot, W. 1984, ApJ, 277, 806
Calvet, N., Hartmann, L. W., & Strom, S. E. 2000, in Protostars and Planets IV, ed. V. Mannings, A. P. Boss, & S. S. Russell (University of Arizona Press, Tuscon), 377
Cassen, P. 1994, Icarus, 112, 405
Crovisier, J., & Bockelée-Morvan, D. 1999, Space Sci. Rev., 90, 19
Crovisier, J., Leech, K., Bockelée-Morvan, D., et al. 1997, Science, 275, 1904
Crovisier, J., Leech, K., Bockelée-Morvan, D., et al. 1999, Workshop on Thermal Emission Spectroscopy and Analysis of Dust, Disks, and Regoliths, April 28-30, 1999, Houston, Texas, abstract No. 3010
Cyr, K. E., Sears, W. D., & Lunine, J. I. 1998, Icarus, 135, 537
D'Alessio, P., Cantò, J., Calvet, N., et al. 1998, ApJ, 500, 411
Draine, B. T. 1985, ApJS, 57, 587
Draine, B. T., & Lee, H. M. 1984, ApJ, 285, 89
Drouart, A., Dubrulle, B., Gautier, D., et al. 1999, Icarus, 140, 129
Dubrulle, B. 1993, Icarus, 106, 59
Duschl, W. J., Gail, H.-P., & Tscharnuter, W. M. 1996, A&A, 312, 624
Fabian, D., Jäger, C., Henning, Th., et al. 2000, A&A, 364, 282
Fegley, Jr. B., & Prinn, R. G. 1989, in The Formation and Evolution of Planetary Systems, ed. H. A. Weaver, & L. Danley (Cambridge University Press), 171
Finocchi, F., & Gail, H.-P. 1997b, A&A, 327, 825
Finocchi, F., Gail, H.-P., & Duschl, W. J. 1997a, A&A, 325, 1264
Gail, H.-P. 1998, A&A, 332, 1099
Gail, H.-P. 2001a, A&A, 378, 192
Gail, H.-P. 2001b, A&A, in press
Hallenbeck, S. L., Nuth III, J. A., & Daukantas, P. L. 1998, Icarus, 131, 198
Hallenbeck, S. L., Nuth III, J. A., & Nelson, R. N. 2000, ApJ, 535, 247
Hanner, M. S., Gehrz, R. D., Harker, D. E., et al. 1997, Earth, Moon and Planets, 79, 247
Hanner, M. S., Hackwell, J. A., Russel, R. W., et al. 1994a, Icarus, 112, 490
Hanner, M. S., Lynch, D. K., & Russel, R. W. 1994b, ApJ, 425, 274
Hartmann, L., & Kenyon, S. J. 1996, ARA&A, 34, 207
Hartmann, L., Calvet, N., Gullbring, E., et al. 1998, ApJ, 495, 385
Hirschfelder, J. O., Curtiss, C. F., & Bird, R. B. 1964, Molecular Theory of Gases and Liquids (Wiley, New York)
Kley, W., Papaloizou, J. C. B., & Lin, D. N. C. 1993, ApJ, 416, 679
Koike, C., Kaito, C., Yamamoto, T., et al. 1995, Icarus, 114, 203
Launder, B. E. 1976, in Turbulence, ed. P. Bradshaw (Springer Verlag, Berlin), 231
Lenzuni, P., Gail, H.-P., & Henning, T. 1995, ApJ, 447, 848
Lichtenegger, H. I. M., & Kömle, N. I. 1991, Icarus, 90, 319
Lide, R. D. 1995, CRC Handbook of Chemistry and Physics, 78th ed. (CRC Press, Boca Raton etc.)
Lin, D. N. C., & Papaloizou, J. C. B. 1980, MNRAS, 191, 37
Lin, D. N. C., & Papaloizou, J. C. B. 1985, in Protostars and Planets II, ed. D. C. Black, & M. S. Matthews (University of Arizona Press, Tucson), 981
Mathis, J. S., Rumpl, W., & Nordsieck, K. H. 1977, ApJ, 217, 425
McComb, W. D. 1990, The Physics of Fluid Turbulence (Oxford Science Publ.)
Morfill, G. E. 1983, Icarus, 53, 41
Morfill, G. E. 1985, in Birth and Infancy of Stars, ed. R. Lucas R., A. Omont, & R. Stora (Elsevier Science Publishers), 693
Morfill, G. E., Tscharnuter, W., & Völk, H.-J. 1985, in Protostars and Planets II, ed. D. C. Black D. C., & M. S. Matthews (University of Arizona Press, Tucson), 493
Morfill, G. E., & Völk, H.-J. 1984, ApJ, 287, 371
Nakamoto, T., & Nakagawa, Y. 1995, ApJ, 445, 330
Natta, A. 2000, in Infrared space astronomy to-day and to-morrow, ed. F. Casoli, F. David, & J. Lequeux (Springer Verlag), 193
Nuth III, J. A., & Donn, B. 1982, ApJ, 257, L103
Pringle, J. E. 1981, ARA&A, 19, 137
Ruden, S. P., & Lin, D. N. C. 1986, ApJ, 308, 883
Ruden, S. P., & Pollack, J. B. 1991, ApJ, 375, 740
Shakura, N. I., & Sunyaev, R. A. 1973, A&A, 24, 337
Shu, F. H., Tremaine, S., Adams, F. C., et al. 1990, ApJ, 358, 495
Stepinski, T. F. 1998, ApJ, 507, 361
Stevenson, D. J. 1990, ApJ, 348, 730
Stevenson, D. J., & Lunine, J. I. 1988, Icarus, 75, 146
Strom, S. E., Edwards, S., & Skrutskie, M. F. 1993, in Protostars and Planets III, ed. E. H. Levy, & J. I. Lunine (University of Arizona Press, Tuscon), 837
Toriumi, M. 1989, Earth and Planetary Science Letters, 92, 265
Waldmann, L. 1958, in Encyclopedia of Physics Vol. XII, ed. S. Flügge (Springer, Berlin), 295
Webb, R. A., Zuckerman, B., Platais, I., et al. 1999, ApJL, 512, 63
Weidenschilling, S. J., & Cuzzi, J. N. 1993, in Protostars and Planets III, ed. E. H. Levy, & J. I. Lunine (University of Arizona Press, Tuscon), 1031
Weinberger, A. J., Becklin, E. E., Schneider, G., et al. 2002, ApJ, 566, 409
Weingartner, J. C., & Draine, B. T. 2001, ApJ, 548, 296
Yanamandra-Fisher, P. A., & Hanner, M. S. 1999, Icarus, 138, 107